PCCP
Physical Chemistry Chemical Physics

Accepted Manuscript

This article can be cited before page numbers have been issued, to do this please use: A. Mandal, C. Mohn, Y. Chanchangi and C. H. Gorbitz, *Phys. Chem. Chem. Phys.*, 2026, DOI: 10.1039/D6CP00757K.

ROYAL SOCIETY OF CHEMISTRY

rsc.li/pccp

View Article Online
DOI: 10.1039/D6CP00757K

DFT insights into opto-electronic properties of near infra-red absorber 1:1 perylene:TCNQ cocrystal towards photovoltaic application

Arkalekha Mandal,[a*] Chris Erik Mohn[a], Yusuf Chanchangi,[b] Carl Henrik Görbitz[a]

[a] Department of Chemistry, Blindern Campus, University of Oslo, Oslo 0371, Norway

[b] Environmental and Sustainability Institute, Faculty of Environment, Science and Economy, University of Exeter, Exeter, Penryn Campus, Cornwall TR10 9FE, United Kingdom

Abstract

With the advent of photovoltaic materials with room temperature solution processing ability and light-weightiness, organic materials have emerged as a particular promising family of candidates. Organic cocrystals comprising π-electron rich donor and π-electron deficient acceptor hold immense potential within the field of thin film photovoltaic devices possessing strong and broad optical absorption covering the visible and near infra-red region of solar spectrum, intrinsic semiconductor property, and the solution processing ability at ambient conditions. Still they are strongly under-represented as materials for photovoltaic devices. Herein, we have investigated the excited state features and electron/hole transport properties of 1:1 cocrystal of π-donor perylene and π-acceptor 7,7′,8,8′-tetracyanoquinodimethane (TCNQ). The donor and acceptor molecules form infinite π-stacks via strong face to face π··π staking interaction to facilitate charge transfer. The absorption spectrum of this cocrystal shows quite broad absorption from the UV to the near infrared regions (320-1150 nm) owing to charge transfer. Time dependent DFT study indicates an efficient charge transfer exciton generation and dissociation. The bandgap (0.92 eV) and the exciton binding energy (0.12 eV) values of this cocrystal are ideal for the photovoltaic applications, while the theoretically calculated spectroscopic limited maximal efficiency (SLME) is 24 % at 1000 nm thickness pointing to future applicability. The electron (45 meV) and hole (48 meV) transfer integral values along the π··π stacking direction indicate ambipolar charge transport, while low values of the internal reorganization energy of perylene (147 meV) and TCNQ (255 meV) are favourable for the fast transport of charge carriers making the cocrystal a suitable candidate for photovoltaic applications. The 1:1 perylene:TCNQ cocrystal poses an intriguing example of indirect bandgap organic material having high value of the theoretical maximum photovoltaic efficiency at low film thickness, owing to very similar values of indirect bandgap and

View Article Online
DOI: 10.1039/D6CP00757K

direct allowed bandgap. This theoretical study unveils the photo-physical and charge transport properties of an organic cocrystal with strong potential for photovoltaic applications.

Introduction

In the last two decades, the organic molecular crystals have gained the recognition as potential photovoltaic materials.[1-2] Rubrene,[3] pentacene,[4] and fullerene[5] based molecular crystals have been explored as organic photovoltaic materials as they exhibit strong photon absorption and excellent charge carrier mobility values. However, these materials are known for the limited solubility and hence procuring good quality thin films of these materials is often cumbersome.[6] Recently, a number of non-fullerene small molecules have emerged as the acceptors for bilayer or bulk heterojunction solar cells.[7-11] Addition of alkyl substituents in the molecular backbones help to solve the solubility issue in these non-fullerene acceptors. On the other hand, the heterojunction solar cells are more complicated in fabrication and poor interface morphology of the donor-acceptor interface often reduces the overall photo-conversion efficiency due to charge traps.[12-13] In this regard, organic ambipolar molecular crystals can be the best candidates as integration of both *p*-type and *n*-type semiconductor behaviour in single material and minimal charge traps in crystalline domain will aid in good photovoltaic behaviour.[14-15]

Ambipolar semiconductor property is very rare in organic semiconductors as the majority of the organic molecular semiconductors are *p*-type[16-18] while few molecular semiconductors are *n*-type in nature.[19-20] The promising attempt to secure ambipolar semiconductor property in organic systems was achieved by assembling the π-donor and π-acceptor moieties together in a single component structure via either polymerization[21-22] or cocrystallization.[23] Cocrystallization of π-donor (D) and π-acceptor (A) molecules is the most viable and the least tedious method for procuring ambipolar organic semiconductors with good solution processing ability.[23-26] Ambipolar organic donor acceptor cocrystals with the bandgap in the range of 1.0 to 1.8 eV, strong photon absorption in the visible and near infra-red region of solar spectrum, facile exciton generation and dissociation abilities, and balanced electron and hole transport will be the attractive choices for the thin film organic photovoltaic materials.[28-29]

View Article Online
DOI: 10.1039/D6CP00757K

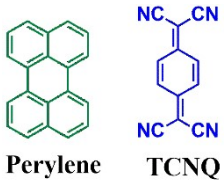

Scheme 1. The donor and acceptor molecules in the studied 1:1 cocrystal.

In the present work we have explored the electronic and charge carrier transport properties of a 1:1 donor acceptor cocrystal comprised of perylene donor and 7,7′,8,8′-tetracyanoquinodimethane (TCNQ) acceptor in both ground and optically excited states (Scheme 1). Perylene is a polycyclic aromatic hydrocarbon (PAH) donor known for being the component of numerous organic cocrystals with remarkable semiconductor[30-31] and fluorescent[32-34] properties. On the other hand, the π-acceptor TCNQ is a widely used molecule to impart *n*-type and ambipolar semiconductor property both in organic cocrystals[35-37] and metal organic frameworks.[38-39] Cocrystallization of perylene and TCNQ to produce 1:1, 3:1 and 3:2 cocrystals have been reported.[40-41] The charge carrier transport properties of the 1:1 perylene:TCNQ cocrystal have been studied experimentally by field effect transistor fabrication and electron mobility values in the range of 0.001-0.01 $cm^2V^{-1}s^{-1}$ were reported.[41] The excited state and photovoltaic properties of 1:1 perylene:TCNQ cocrystal have not been explored so far. The complementarity of molecular electrostatic potential (MEP) of perylene and TCNQ indicate efficient π···π stacking interaction (Figure 1a). In addition, the small energy difference (≈ 0.14 eV) between perylene HOMO and TCNQ LUMO (Figure 1b) will lead to efficient charge transfer. We envisage that the 1:1 perylene:TCNQ cocrystal can impart excellent photovoltaic property owing to both strong face to face π···π stacking between perylene and TCNQ, and facile charge transfer suitable for absorption in the red and infra-red region of the solar spectrum.

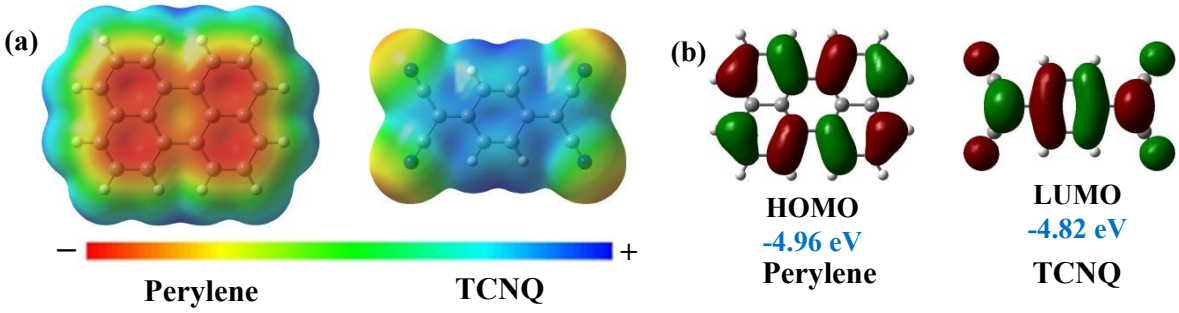

View Article Online
DOI: 10.1039/D6CP00757K

Figure 1. (a) Molecular electrostatic potential of perylene and TCNQ calculated at B3LYP/6-31G(d,p) level in gas phase; (b) energies of HOMO of perylene and LUMO of TCNQ calculated at B3LYP/6-31G(d,p) level of theory on optimized gas phase geometries.

It is known that charge transfer leads to efficient absorption in the visible and near infra-red region for facile exciton generation, while the already reported charge carrier transport property of the 1:1 perylene:TCNQ cocrystal is inductive for photovoltaic property. In current work, we will investigate the excited state and ambipolar charge transport features of the 1:1 perylene:TCNQ cocrystal towards the possibility of photovoltaic application.

Materials and methods

Synthesis of 1:1 perylene:TCNQ cocrystal

The 1:1 perylene:TCNQ cocrystal (literature reported, CCDC number: 1576698) was synthesized by grinding equi-molar amount of perylene (50 mg, ≈ 2 mmol) and TCNQ (40 mg, ≈ 2 mmol) with repetitive additions of 0.5 mL of toluene at 5 minutes interval. The resultant dark green powder was dissolved in 5 mL chlorobenzene and kept undisturbed at room temperature for slow evaporation. Long prismatic blackish green crystals were grown after a week (Figure S2 in SI). The mechano-chemical cocrystal synthesis was opted for green chemistry approach.

Spectroscopic characterization

The single crystals of 1:1 perylene:TCNQ cocrystal (50 mg) were collected and dissolved in 10 mL of chlorobenzene. Solid polymethylmacrylate (PMMA) polymer (50 mg) was dissolved in 10 mL chlorobenzene at 50° C. The solution of the cocrystal was poured into the solution of PMMA, and the mixed solution was stirred for few minutes. The mixed solution was then drop-casted on glass slides, and annealed at 60° C for making a yellow coloured drop-casted thin films. The PerkinElmer LAMBDA 1050+ UV/Vis/NIR Spectrophotometer was employed to collect spectral absorbance and transmittance data. The instrument was operated in absorbance mode, with the data recorded at 5 nm intervals across a wavelength range from 300 to 1800 nm, encompassing the ultraviolet (UV), visible (Vis), and near-infrared (NIR) regions. The optical bandgap of the cocrystal has been determined from Tauc plot which is widely used for the amorphous (powder) or disordered (solution processed thin film) materials. The photon energy (*hv*) is plotted along the

View Article Online
DOI: 10.1039/D6CP00757K

x-axis while the quantity $(\alpha hv)^{1/2}$ (for indirect bandgap) or $(\alpha hv)^2$ (for direct bandgap) is plotted along the y-axis, with α being the absorption coefficient of the material. Extrapolation of the curve along the abscissa produces the optical bandgap energy of the semiconductor material.

Computational methods

Theoretical estimation of intermolecular interaction energies

The binding energy between the π-stacked or weak hydrogen bonded donor and acceptor moieties in the gas phase dimer was calculated at the crystal structure (literature reported, CCDC number: 1576698) geometry using Grimme's dispersion with Becke-Johnson damping corrected B3LYP functional (B3LYP-D3-BJ) and 6-31G(d,p) basis set. The counterpoise method was used to correct the basis set superposition error (BSSE) as we used a relatively small basis set for calculating the intermolecular interaction energy.[42] The binding energy values corresponding to π···π stacking and hydrogen bonding interactions in solid state were calculated at the B3LYP/6-31G(d,p) level of theory using CrystalExplorer.[43-44]

Theoretical prediction of opto-electronic properties at molecular level

The Gaussian 16 program package was used for all calculations at the atomic level. The HOMO/ LUMO energies and molecular electrostatic potential surfaces of the donor and acceptor molecules were calculated at B3LYP/6-31G(d,p) level of theory. The HOMO/LUMO energies of D–A dimer, A–D–A–D tetramer, and A–D–A–D–A–D hexamer were calculated by the Grimme's dispersion (D3)[45] corrected B3LYP functional with 6-31G(d,p) basis set, using the atomic coordinates extracted from the literature reported room temperature crystal geometry. The Becke Johnson damping function was used along with dispersion corrected D3 functional.[46] The donor to acceptor charge transfer is quantified from the Natural bond orbital (NBO)[47] analysis of the π-stacked perylene–TCNQ dimer performed Grimme's dispersion (D3) corrected B3LYP functional. The second order perturbation (E^2) energy[48] values for electron transfer from the filled π-orbitals on perylene to the empty π*-orbitals on TCNQ, along with the NBO atomic charges on these moieties give an estimation of charge transfer from perylene to TCNQ.

To calculate the excited state properties time dependent DFT (TD-DFT) calculations on the D–A dimer, and A–D–A–D tetramer were performed using the experimental coordinates from literature reported crystal structure. The CAM-B3LYP functional[49-50] was used for TD-DFT calculation, and

View Article Online
DOI: 10.1039/D6CP00757K

only spin allowed singlet-singlet transitions were considered for the optically excited states. The range separated exchange-correlation functional CAM-B3LYP with 19% Hartree-Fock exchange at short range, 65% Hartree-Fock exchange at the long-range (> 10 Å) and 33% HF (HF) exchange in the intermediate range, takes account of long range electron-electron coupling effect in π-stacked D–A systems to produce reliable transition energy values. The electron-hole distribution, coefficient of electron-hole mixing,[51] charge transfer length,[52] and one electron transition density matrix[52] for the excited states were obtained from the TD-DFT calculation results. The Mutltiwfn software[51-52] was used for plotting the excited state electron-hole distribution maps, heat maps for one electron transition density matrix, as well as, calculating the charge transfer lengths and electron-hole mixing coefficient. Another range-separated hybrid functional ω97X-D was used to calculate the excited state properties of π-staked D–A dimer and A–D–A–D tetramer, and the values of different parameters were compared with those obtained by the CAM-B3LYP functional. The range separated ωB97X-D functional is comprised of 22% Hartree Fock exchange at short range and 100% Hartree Fock exchange at long range, while the intermediate region is defined with a standard error function with range separation parameter value of 20%.[54]

Modelling of charge carrier transfer:

The internal hole/electron reorganization energy (λ_{int}) of donor and acceptor molecules were calculated at B3LYP/6-31G(d,p) level by adding the molecular reorganization energy at both the neutral ground (λ_i) and charged excited (λ_f) states upon the molecular cation/anion formation. A four point energy model[55] was followed to estimate the value of internal reorganization energy (λ_{int}) of the molecules;

$\lambda = \lambda_i + \lambda_f = (E^{**}_{cation/anion} - E_{neutral}) + (E^{*}_{cation/anion} - E_{cation/anion})$ Equation (1),

$\lambda_i = (E^{**}_{cation/anion} - E_{neutral})$, and $\lambda_f = (E^{*}_{cation/anion} - E_{cation/anion})$.

The $E_{neutral}$ and $E_{cation/anion}$ terms indicate the energies of the optimized geometry of neutral molecule and optimized geometry of the cation/anion. On the other hand, the $E^{*}_{cation/anion}$ and $E^{**}_{cation/anion}$ terms refer to the single point energy of the cation/anion with the optimized geometry of neutral state of molecule and the single point energy of the neutral molecule with the optimized geometry of cationic/anionic states respectively.

View Article Online
DOI: 10.1039/D6CP00757K

The super-exchange and direct electron and hole transfer integrals were calculated at the CAM-B3LYP/6-31G(d,p) level of theory. The long range corrected CAM-B3LYP functional was used for the transfer integral calculation as the frontier molecular orbitals in the non-covalently bonded molecular dimers (D–D/A–A) or π-stacked trimers (A–D–A/ D–A–D) are generally distributed on two different molecules. Hence transfer integral calculation necessitate the long range electron correlation for calculating the energy of molecular orbitals distributed on multiple molecules.

Band structure calculation

The band structure calculation for perylene:TCNQ cocrystal was performed both at reported room temperature (290 K) experimental and optimized unit cell geometries using Vienna *ab initio* simulation package (VASP, version 6.4.3). The geometry optimization was performed with van der Waals density functional (vdW-DF) with an energy cut-off 700 eV and a convergence criterion 10^{-7} eV/Å for the calculation of total energies. A Γ-centered 4×3×2 mesh of k-points and Gaussian smearing with smearing width 0.03 eV were used for the optimization of the unit cell volume, shape and basic atomic positions. The van der Waals density functional has been used for optimization as the crystal packing of the cocrystal is dominated by van der Waals type π··π and C–H··π interactions. The unit cell parameters from the experimental and optimized geometries are listed as the following; experimental: a = 7.30 Å, b = 10.87 Å, c = 14.55 Å; optimized with VdW-DF: a = 7.50 Å, b = 10.90 Å, c = 14.52 Å.

Band structure calculations on the experimental and DFT optimized geometries were performed with an energy cut-off of 500 eV and a Monkhorst-pack 5×3×2 mesh of k-points for the SCF total energy calculation and a density of k-points equal to 0.06/ Å between the high symmetry points to draw the band structure. A convergence criterion of 10^{-7} eV/Å for the electronic wave-function were applied to calculate the band structure using the hybrid DFT functional HSE06. The HSE06 functional has been recognized to give accurate value of the band structure for organic systems.[56-57] A Gaussian smearing scheme with a smearing width 0.02 eV was used for band structure calculations. The band structure calculation for 1-aminopyrene:TCNQ cocrystal (CCDC: 1915543) was performed using the experimental geometry using the HSE06 functional, while geometry optimization was performed for CBP:$(TCNQ)_2$ (CBP = π-donor 4,4′-bis(carbazol-9-yl)biphenyl) cocrystal (CCDC: 2058993). The C17, C18, H17, H18 atoms of the CBP:$(TCNQ)_2$ cocrystal have 80:20 occupancies distributed over two positions. We considered full occupancies

View Article Online
DOI: 10.1039/D6CP00757K

at the atomic sites with experimental 80 % occupancy and removed atomic sites with 20 % occupancy manually to carry out the geometry optimization. The van der Waals density functional (vdW-DF) with an energy cut-off 600 eV, Γ-centered 2×2×1 mesh of k-points, and a convergence criterion 10^{-7} eV/Å for optimization of basic atomic positions keeping the unit cell geometry fixed. The VASPKIT software (version 1.3.5) was used for post processing of all the data including calculation of spectroscopy limited maximum efficiency (SLME) parameter required for photo-conversion property evaluation. The SLME parameter η value equals to P_m/P_{in}, where P_m = maximum power density obtained from the material and P_{in} = incident power density from the solar spectrum. The η value is extracted by using an exponential function to model the fraction of radiative recombination as stated in the following equation:

$J_{SC} = J_0 exp \int_0^\infty a(E) Isun E dE$ Equation (2);

while the parameters J_{SC} = Photo-voltaic current, a(E) = Photon absorptivity, I_{sun} = AM 1.5 G solar spectrum (wavelength range 280-2000 nm), J_0 = reverse photo-current which depends on both the radiative and non-radiative recombination in the dark state.

The expression of $J_0 = J_0^r + J_0^{nr} = J_0^r / exp(E_g - E_g^{da}/kT)$ Equation (3);

while E_g = fundamental bandgap and E_g^{da} = direct allowed bandgap. Consequently, the SLME value tends to zero for indirect bandgap materials if difference between the direct allowed and fundamental bandgap becomes large. In contrast, the SLME parameter gives fairly comprehensive idea of theoretical maximum photo-conversion efficiency for the direct bandgap materials, and also for the indirect bandgap materials with considerably small difference between the indirect bandgap and the direct allowed bandgap. The SLME parameter gives more practical estimation of accurate efficiency compared to the traditional Shokley-Queisser (SQ) limit which only takes in account of the radiative charge carrier recombinations.[58] In contrast, the SLME parameter takes account of both radiative and non-radiative recombination, and provides a comprehensive idea on the photo-conversion efficiency.

Results and discussion

Crystal packing of 1:1 perylene TCNQ cocrystal

The 1:1 perylene:TCNQ cocrystal (Figure S1 in SI) is crystallized in centro-symmetric monoclinic space group $P2_1/c$. The asymmetric unit contains half molecule of perylene and half molecule of

View Article Online
DOI: 10.1039/D6CP00757K

TCNQ, and two such asymmetric units are present in the unit cell. The perylene and TCNQ molecules are tethered in an infinite chain along the crystallographic *a* axis via strong face to face π··π stacking interaction. The distance between the centroids (Cg) of the 20-member aromatic core of perylene and the 6-membered quinonoid core of TCNQ is 3.469 Å, while the angle between these planes is 4.40° (Figure 2a). The infinite ··D–A–D–A·· molecular stacks present in the crystal packing (Figure 2b, Table 1) are adjoined by C9–H9··N1 (C··N, 3.431(2) Å; C··N, 2.71 Å, and C–H··N, 134.8°) hydrogen bond along the crystallographic *c* axis, and by C7–H7··N2 (C··N, 3.523(3) Å; C··N, 2.67 Å, and C–H··N, 153.3°) hydrogen bond along the crystallographic *b* axis (Figure 2c, Table 1).

The strength of the intermolecular interactions were estimated both in the gaseous and solid phase using the experimentally observed coordinates of the molecular dimers. The binding energy of the face to face π··π stacking interaction in the gas phase and solid state is -21.98 and -15.02 kcal/mol respectively. The strength of the C–H··N hydrogen bonds in the gas phase are -1.58 and -2.19 kcal/mol, which is significantly less in comparison to the strength of π··π stacking interaction. This indicates that π··π stacking is the major attractive non-covalent interaction in the crystal packing and points to the direction of charge carrier transport.

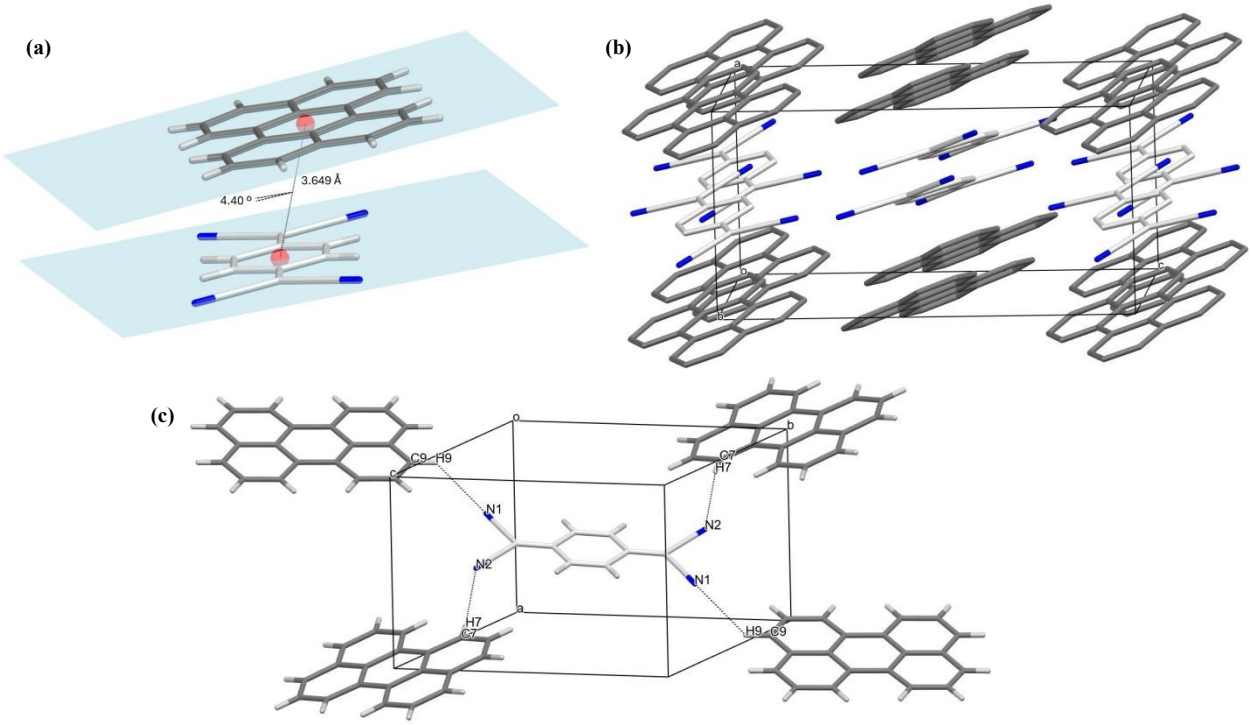

View Article Online
DOI: 10.1039/D6CP00757K

Figure 2. (a) The parameters of face to face π··π stacking between the donor and acceptor; (b) molecular stacks formed by alternative perylene and TCNQ molecules; (c) the C–H··N hydrogen boding interactions between the perylene and TCNQ molecules from different π-stacks leading to three dimensional crystal packing, the carbon atoms of perylene and TCNQ molecules are coloured differently for visualization purpose.

Table 1. Non-covalent interaction parameters observed in crystal packing of 1:1 perylene:TCNQ cocrystal

Interaction	D··A (in Å)	H··A (in Å)	D–H··A (in °)	Symmetry
π··π stacking				x, y, z
C9–H9··N1	3.431(2)	2.71	134.8	1-x, 1-y, 1-z
C7–H7··N2	3.523(3)	2.67	153.3	x, y, z

Ground state electronic property of 1:1 perylene:TCNQ cocrystal

The frontier molecular orbital analyses on perylene:TCNQ cocrystal have been carried out with both Grimme's D3-dispersion corrected B3LYP functional with Becke-Johnson damping factor (B3LYP-D3-BJ) and range separated CAM-B3LYP functional. The HOMO-LUMO difference is observed as 1.68 eV by B3LYP functional with D3-BJ dispersion correction, while this value is obtained as 3.3 eV by CAM-B3LYP functional. In contrast, the geometrical offset of the molecular orbitals is unchanged with the use of DFT-functionals as the HOMO is concentrated on the perylene and the LUMO is located on TCNQ (Figure 3 and S3 in ESI). The HOMO-1 orbital is observed to be primarily located on the acceptor while the HOMO-2 orbital is based on the donor. The LUMO+1 orbital is observed to be fully concentrated on the perylene molecule by CAM-B3LYP calculation (Figure S3 in SI), while the application of B3LYP functional with D3-BJ dispersion produces the LUMO+1 orbital mainly located on TCNQ molecule (Figure 3). Frontier molecular orbital of D–A–D–A tetramer were analyzed at B3LYP-D3-BJ/6-31G(d,p) level of theory (Figure S4-S5) using both CAM-B3LYP and Grimme's D3-dispersion corrected B3LYP functional, and similar geometrical offset for the HOMO and LUMO were observed with the HOMO/LUMO energy difference of 1.23 eV by the B3LYP-D3 functional. In contrast, the HOMO/LUMO energy difference in π-stacked hexameric D–A–D–A–D–A unit calculated by B3LYP-D3/6-31G(d,p) level of theory is 1.38 eV (Figure S6 in SI).

View Article Online
DOI: 10.1039/D6CP00757K

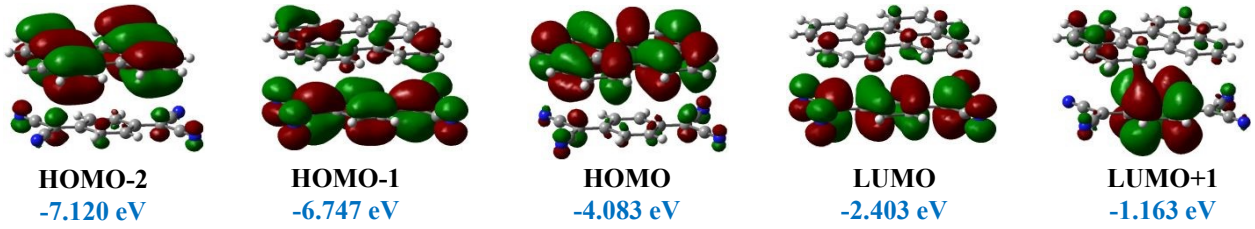

Figure 3. Frontier molecular orbitals of D–A dimer carried out at B3LYP-D3-BJ/6-31G(d,p) level.

The donor to acceptor charge transfer was confirmed by natural bond orbital (NBO) analyses, and significant values of the second order perturbation energy E^2 (Figure 4). We have also calculated the degree of ground state charge transfer by NBO method as NBO charges are considered to be more accurate than Mulliken charge analysis. The degree of ground state charge transfer is around 0.2 indicating a prominent CT character of the 1:1 perylene:TCNQ cocrystal. This value of degree of charge transfer from our study matches closely with the reported literature.[41a]

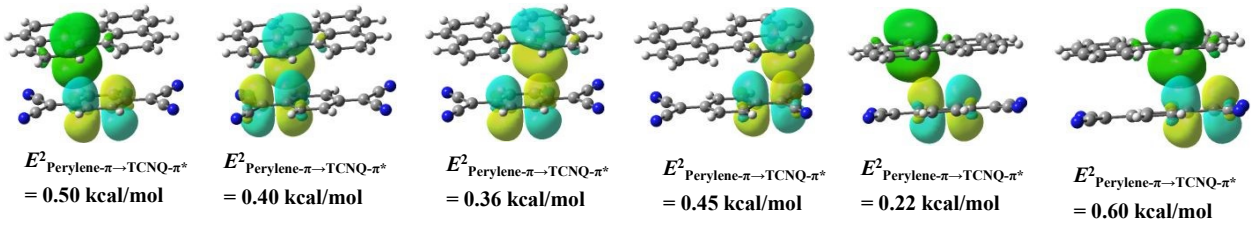

Figure 4. Natural bond orbital analysis on π-stacked D–A dimer, the second order perturbation energy E^2 values indicate significant charge transfer.

Optical and excited state properties of the 1:1 perylene:TCNQ cocrystal

The absorption spectrum of 1:1 perylene:TCNQ cocrystal was recorded in the range 300-1500 nm using drop-casted thin film samples. A broad absorption peak owing to charge transfer is observed spanning from red end of the visible region to near the infra-red region (600-1150 nm). More distinguished shaped and brighter absorption peaks (325-550 nm) are observed in the UV region and the blue-green regions of the visible region (Figure 5).

View Article Online
DOI: 10.1039/D6CP00757K

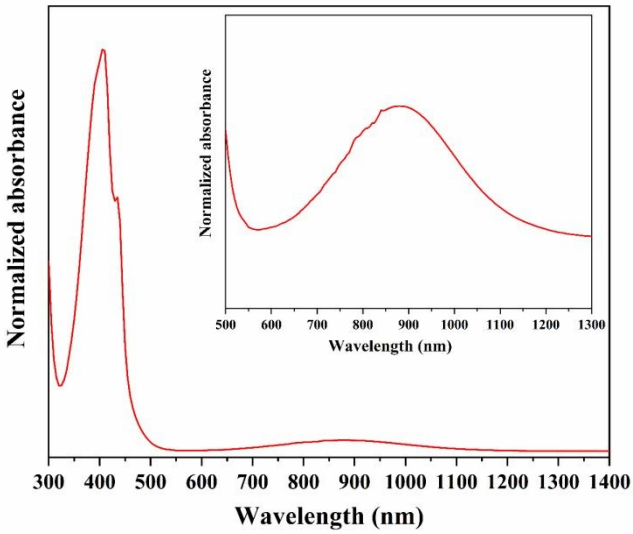

Figure 5. The absorption spectrum of 1:1 perylene:TCNQ corystal drop-casted thin film samples, absorption in the red and infra-red regions are shown as the inset figure.

We have carried out the time-dependent DFT study on π-stacked D–A dimer and D–A–D–A tetramer using two range separated and long range corrected DFT functionals CAM-B3LYP and ω97X-D with 33% and 20% Hartree Fock exchange at the short range respectively. The TD-DFT results obtained by CAM-B3LYP functional on the D–A dimer shows that the $S_0 \rightarrow S_1$ (815 nm, oscillator strength = 0.072) and $S_0 \rightarrow S_3$ (389 nm, oscillator strength = 0.023) transitions (Figure 6, Table 2) have predominant charge transfer nature. In contrast, the $S_0 \rightarrow S_2$ (422 nm, oscillator strength = 0.126) is mainly originated from the intramolecular excitation in the TCNQ molecule.

Table 2. Calculate wavelength, transition energy, oscillator strength and orbital contributions for the $S_0 \rightarrow S_1$, $S_0 \rightarrow S_2$ and $S_0 \rightarrow S_3$ transitions in D–A dimer at CAM-B3LYP/6-31G(d,p) level

Transitions	Wavelength (nm)	Energy (eV)	Oscillator strength	Orbital contribution
$S_0 \rightarrow S_1$	815	1.52	0.0723	HOMO→LUMO, 100%
$S_0 \rightarrow S_2$	422	2.94	0.1260	HOMO-2→LUMO, 2.19% HOMO-1→LUMO, 72.83% HOMO→LUMO+1, 24.98%
$S_0 \rightarrow S_3$	389	3.18	0.0228	HOMO-3→LUMO, 16.65% HOMO-2→LUMO, 67.73% HOMO→LUMO+1, 15.62%

View Article Online
DOI: 10.1039/D6CP00757K

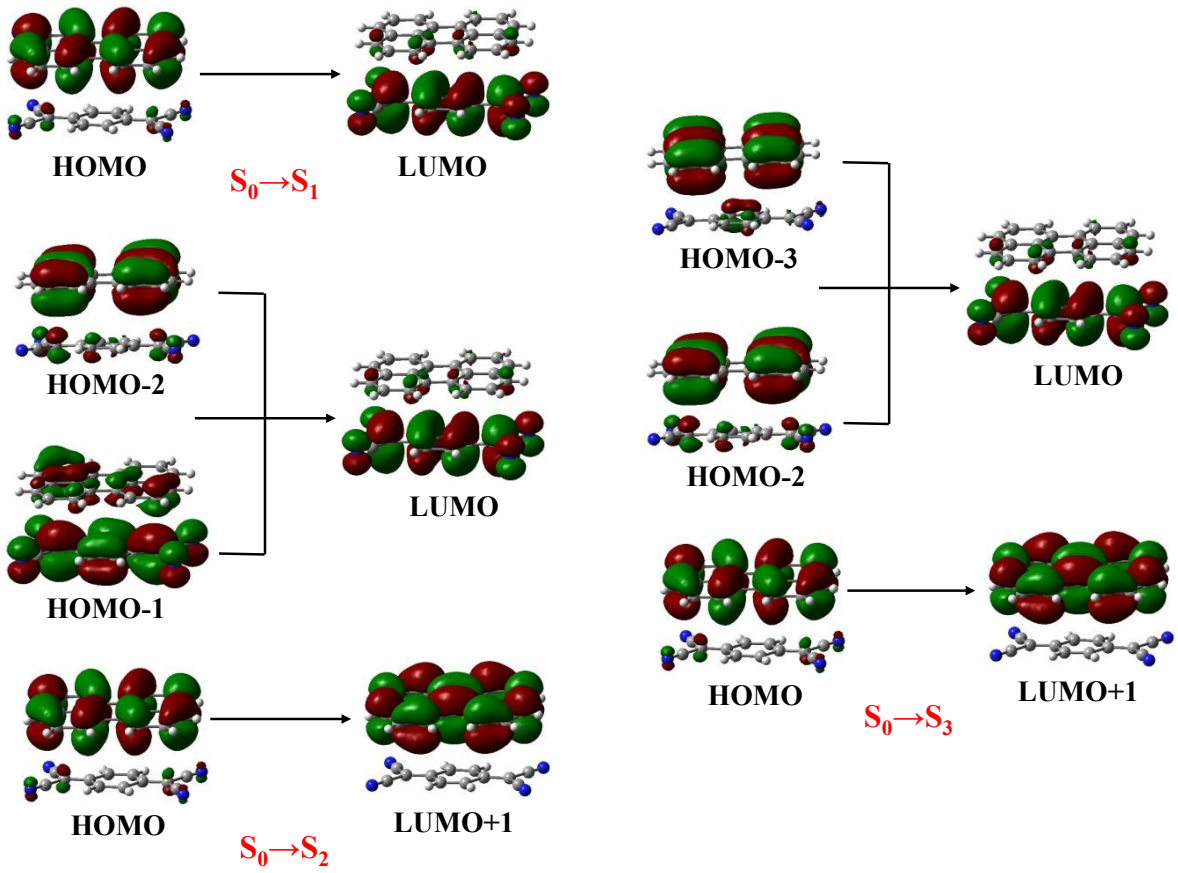

Figure 6. Molecular orbitals taking part in the $S_0 \rightarrow S_1$, $S_0 \rightarrow S_2$ and $S_0 \rightarrow S_3$ transitions of π-stacked D–A dimer, time dependent DFT analysis was carried out CAM-B3LYP/6-31G(d,p) level.

The charge transfer character of the excited state electron hole analysis were further analyzed (Figure 7a). The electron-hole mixing parameter for the excited S_1 and S_3 states are 0.38 and 0.42 respectively indicating substantial charge transfer character of these excite states. The charge transfer length *i.e.*, the length of electron and hole epicenters in the S_1 and S_3 states are 3.38 and 2.81 Å (table 4). On the other hand, the S_2 state (422 nm, oscillator strength = 0.126) has very prominent local excitation character as can be confirmed from the electron hole mixing coefficient being 0.49 and the charge transfer length being 0.84 Å (Table 4). We have performed on electron transition density matrix analysis for the $S_0 \rightarrow S_1$, $S_0 \rightarrow S_2$ and $S_0 \rightarrow S_3$; the heat maps of transition density matrix for the $S_0 \rightarrow S_1$ and $S_0 \rightarrow S_3$ transitions show bright off-diagonal elements confirming the charge transfer character (Figure 7b). The large and very bright off-diagonal elements for the $S_0 \rightarrow S_1$ transition indicates exclusive charge transfer origin. In contrast, the heat map of the electron transition density matrix of $S_0 \rightarrow S_2$ transition is observed with bright diagonal elements

View Article Online
DOI: 10.1039/D6CP00757K

which is indicative of local excitation nature (Figure 7b). Similar results were obtained using ω97X-D functional (Table S2, Figure S7 in SI) which further confirms the charge transfer character of the $S_0 \rightarrow S_1$ and $S_0 \rightarrow S_3$ transitions, and local excitation nature of the $S_0 \rightarrow S_2$ transition.

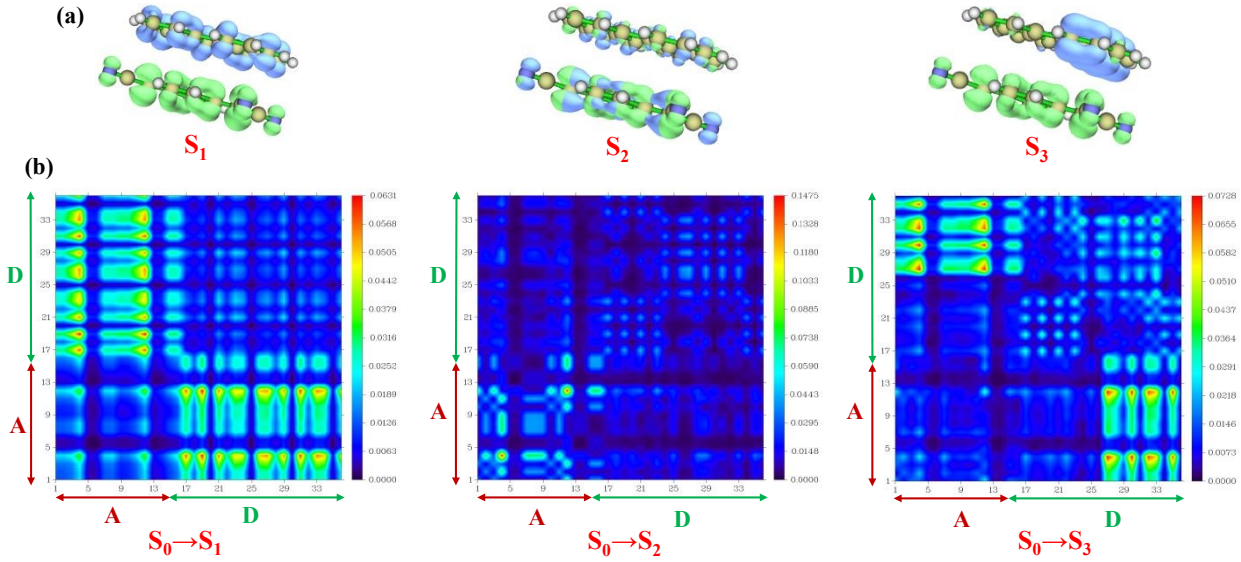

Figure 7. (a) Electron hole distribution maps in the excited states S_1, S_2 and S_3 calculated at CAM-B3LYP/6-31G(d,p) level of theory on π-stacked D–A dimer; (b) the heat maps of one electron transition density matrix for $S_0 \rightarrow S_1$, $S_0 \rightarrow S_2$ and $S_0 \rightarrow S_3$ transitions of π-stacked D–A dimer.

The time dependent analysis was also performed for the π-stacked D–A–D–A tetramer to check the convergence of the calculation results obtained from D–A dimer. The TD-DFT analysis carried out on the tetramer confirms the prominent charge transfer character of $S_0 \rightarrow S_1$ (1.60 nm, oscillator strength = 0.202), and $S_0 \rightarrow S_3$ (640 nm, oscillator strength = 0.037) while the $S_0 \rightarrow S_2$ (750 nm), $S_0 \rightarrow S_4$ (540 nm) are the dark transitions with zero oscillator strength (Table 3, Figure 8). In contrast, the $S_0 \rightarrow S_5$ (432 nm, oscillator strength = 0.046), and $S_0 \rightarrow S_6$ (420 nm, oscillator strength = 0.132) transitions have prominent local excitation character due to intramolecular transitions in TCNQ (Figure 8). We have carried out the excited state and one electron transition density matrix analyses to further confirm the generation of charge transfer excitations upon light absorption. The electron hole distribution analyses for the S_1 and S_3 excited states show prominent geometrical offset with holes concentrated on the donor and the electrons primarily located on the acceptor (Figure 9a), however, considerable electron hole mixing is observed for the S_5 and S_6 states (Figure

View Article Online
DOI: 10.1039/D6CP00757K

9a). The degree of electron hole mixing for the excited S_1, S_3, S_5, and S_6 states are respectively 0.34, 0.37, 0.82 and 0.73 respectively indicating prominent local excitation character of the S_5 and S_6 state. The charge transfer length *i.e.*, the rough estimate of the exciton size corresponding to the S_1 and S_3 states are respectively 7.67 and 6.46 Å and these values confer the possibility of plausible charge transfer excitation dissociation (Table 4).[59] In contrast, the charge transfer lengths for the locally excited S_5 and S_6 states are 0.93 and 3.28 Å respectively (Table 4), and such values are unfavourable for the exciton dissociation.[59-60] The heat maps of the one electron transition density matrix for the $S_0 \rightarrow S_1$ and $S_0 \rightarrow S_3$ transitions demonstrate the bright off-diagonal elements but no diagonal elements, confirming their pure charge transfer origin (Figure 9b). On the other hand, the $S_0 \rightarrow S_5$ and $S_0 \rightarrow S_6$ transition is characterized with only diagonal elements which indicates their local excitation origin.

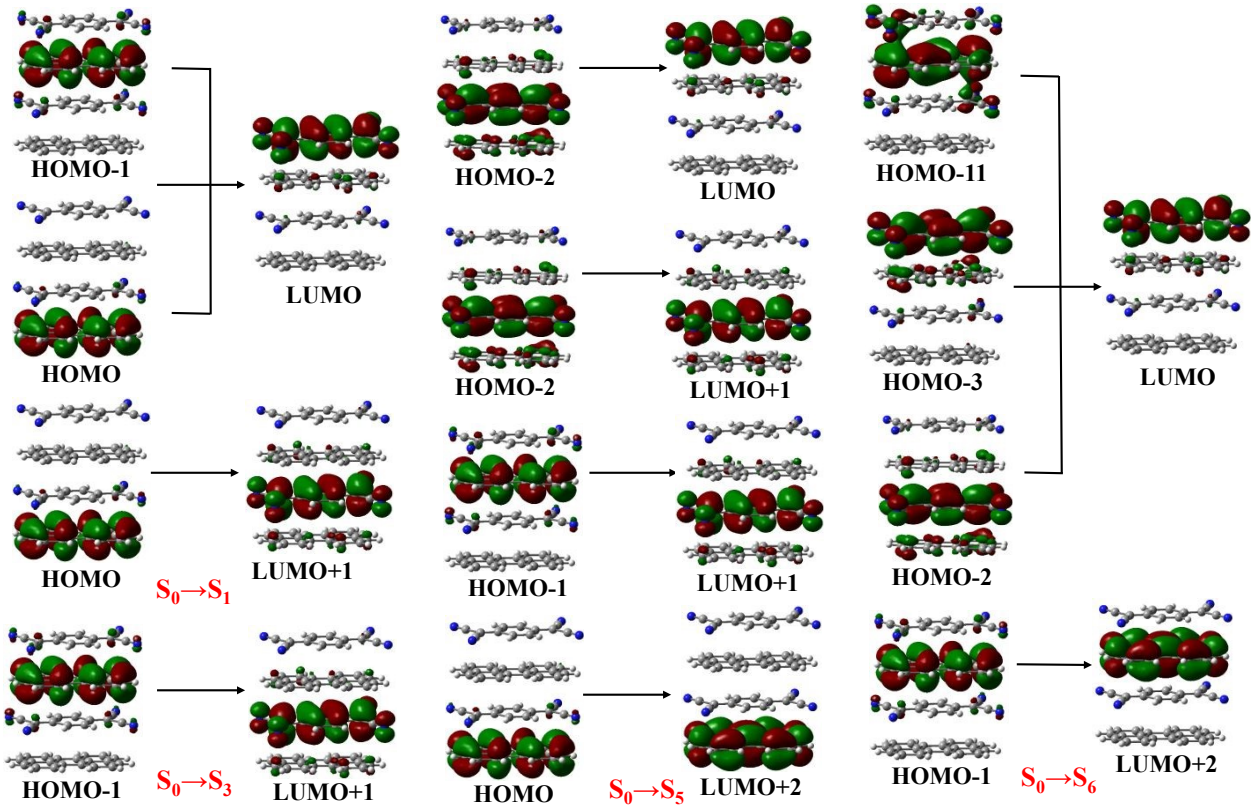

Figure 8. Molecular orbitals taking part in electronic transitions in π-stacked D–A–D–A tetramer, calculations were carried out at CAM-B3LYP/6-31G(d,p) level of theory.

Table 3. Calculate wavelength, transition energy, oscillator strength and orbital contributions for the $S_0 \rightarrow S_1$, $S_0 \rightarrow S_3$, $S_0 \rightarrow S_4$ and $S_0 \rightarrow S_6$ transitions in π-stacked D–A–D–A tetramer at CAM-B3LYP/6-31G(d,p) level of theory

View Article Online
DOI: 10.1039/D6CP00757K

Transitions	Wavelength (nm)	Energy (eV)	Oscillator strength	Orbital contribution
$S_0 \rightarrow S_1$	775	1.60	0.202	HOMO-1→LUMO, 43.86% HOMO→LUMO, 8.11% HOMO→LUMO+1, 48.03%
$S_0 \rightarrow S_3$	639	1.94	0.037	HOMO-1→LUMO+1, 100%
$S_0 \rightarrow S_5$	432	2.87	0.046	HOMO-2→LUMO, 4.74% HOMO-2→LUMO+1, 71.64% HOMO-1→LUMO+1, 9.93% HOMO→LUMO+2, 13.74%
$S_0 \rightarrow S_6$	420	2.95	0.132	HOMO-11→LUMO, 2.34% HOMO-3→LUMO+1, 58.64% HOMO-2→LUMO, 19.35% HOMO→LUMO+1, 19.77%

Table 4. Excited state properties in π-stacked D–A dimer and D–A–D–A tetramer to understand exciton dynamics, calculated at CAM-B3LYP/6-31G(d, p) level of theory

System	Excited state	Charge transfer length (Å)	Electron-hole mixing coefficient
D–A dimer	S_1	3.38	0.38
	S_2	2.81	0.42
	S_3	0.49	0.84

View Article Online
DOI: 10.1039/D6CP00757K

A–D–A–D tetramer	S_1	7.67	0.34
	S_3	6.46	0.37
	S_5	0.93	0.82
	S_6	3.28	0.73

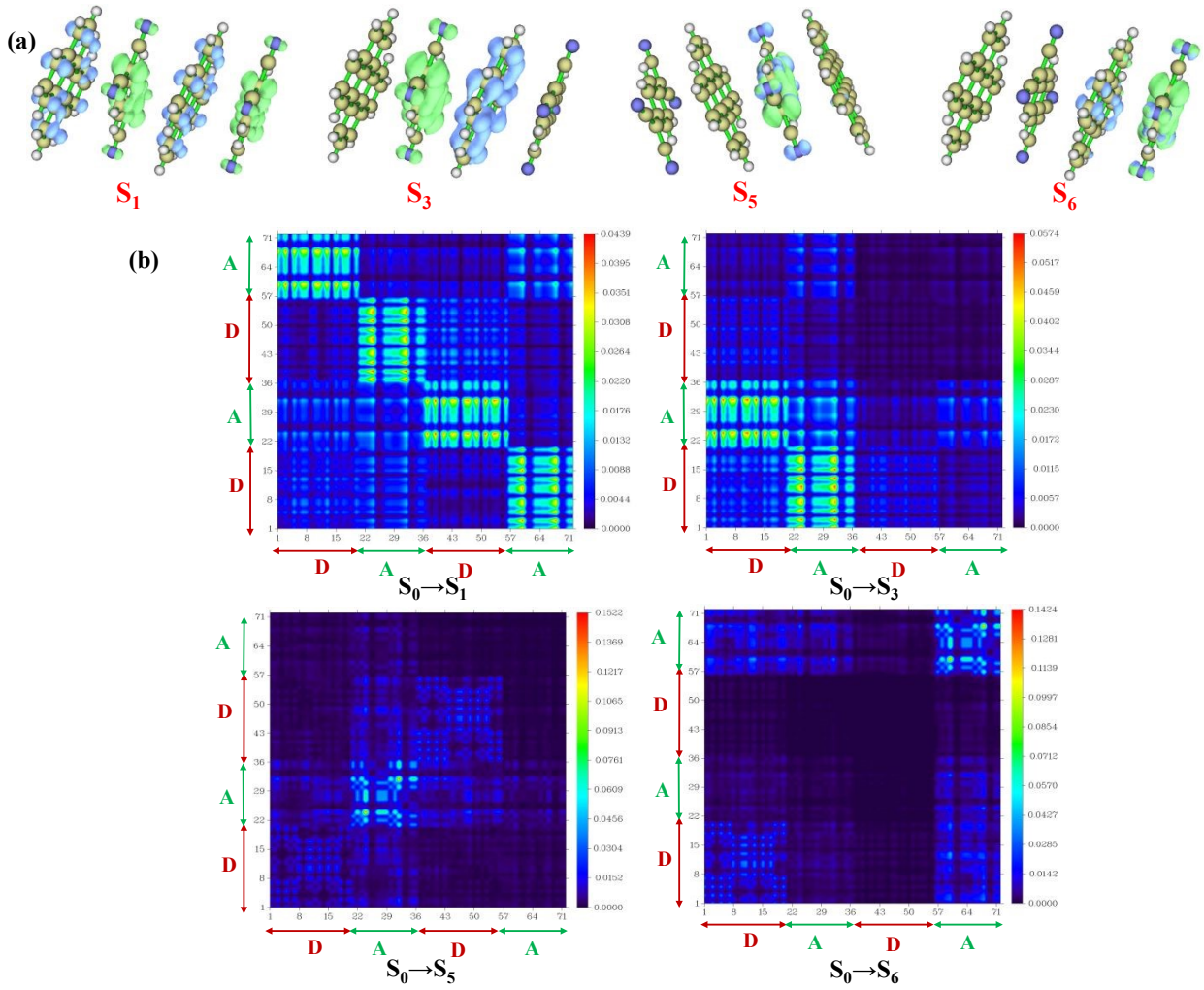

Figure 9. (a) Electron hole distribution in the excited states S_1, S_3, S_5 and S_6 calculated at CAM-B3LYP/6-31G(d,p) level of theory on π-stacked D–A–D–A tetramer; (b) the heat maps of one electron transition density matrix for the $S_0 \rightarrow S_1$, $S_0 \rightarrow S_3$, $S_0 \rightarrow S_5$ and $S_0 \rightarrow S_6$ transitions in the π-stacked D–A–D–A tetramer.

View Article Online
DOI: 10.1039/D6CP00757K

Charge carrier transport in 1:1 perylene:TCNQ cocrystal

The electron and hole transport in molecular semiconductors occur via hopping mechanism. The rate of charge carrier transport k_T via hopping mechanism can be expressed following Marcus-Hush equation[61]:

$$(k_T)\colon k_T = \frac{4\pi^2}{h}\frac{1}{\sqrt{4\pi\lambda k_B T}}\, t^2 exp\left[\frac{-(\Delta G^o+\lambda)^2}{4k_B\lambda T}\right] \quad \text{Equation (4).}$$

The terms *t*, λ, and ΔG° denote transfer integral, reorganization energy, and free energy of electron transfer respectively.

The charge carriers in mixed stack D–A cocrystals can occur via both super-exchange and direct pathways. An electron (or a hole) is transported from the LUMO of one acceptor (or the HOMO of one donor) molecule to the LUMO of consecutive acceptor (or the HOMO of the next donor) molecule via the HOMO of bridging donor (or the LUMO bridging acceptor) molecule. The super-exchange electron integral is calculated by the energy splitting of the LUMO (*i.e.*, LUMO and LUMO+1 orbital) of the π-stacked A–D–A molecular trimer, while the super-exchange hole transfer integral is computed from the energy splitting of the HOMO (*i.e.*, HOMO and HOMO-1 orbital) of the π-stacked D–A–D trimer. In addition, the electron and hole transfer can also take place by direct transfer between the nearest donor or the acceptor molecules.[62-65] The transfer integral values corresponding to direct electron or hole transfer are calculated from the energy splitting of LUMO of the nearest acceptor dimer and the energy splitting of the HOMO of the nearest donor dimer respectively.[66] The reorganization energy (λ) term corresponds the energy requirement due to change in geometry of a molecule and its surroundings when it accepts or ejects an electron (*i.e.*, hole formation). The total reorganization energy is a sum of internal (λ_{int}) or external (λ_{ext}) terms. The λ_{int} presents the energy required for the change in molecular geometry upon $D^{\cdot+}$ or $A^{\cdot-}$ formation from neutral D/A molecule, while the energy required for the change in the geometries of surrounding molecules is expressed by λ_{ext} term.[67]

View Article Online
DOI: 10.1039/D6CP00757K

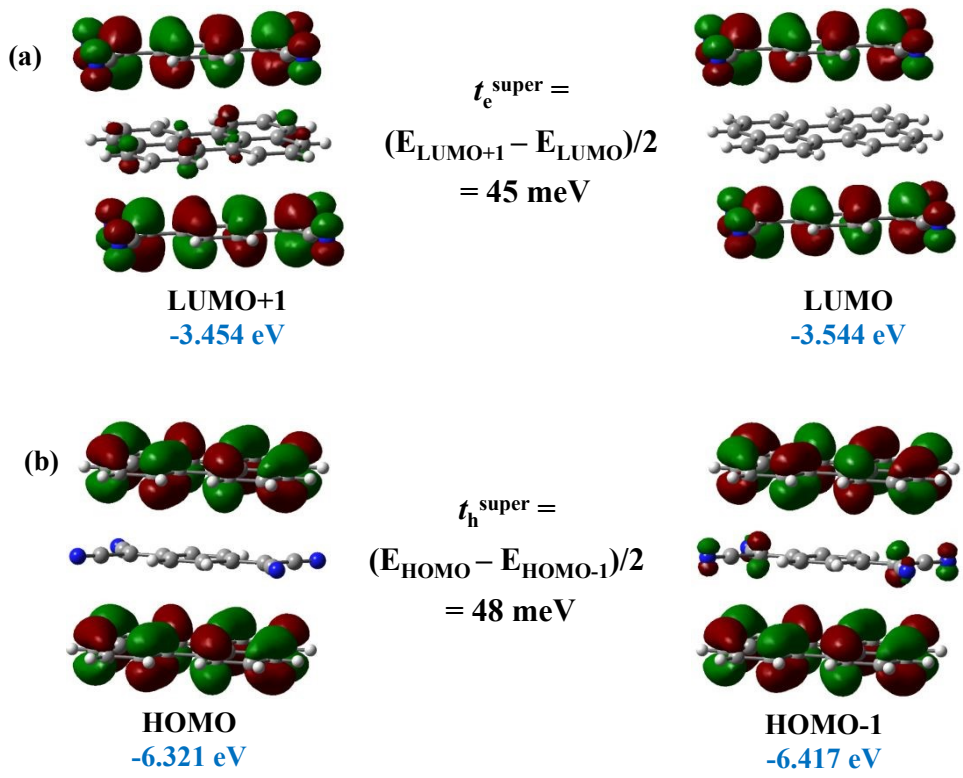

Figure 10. (a) Super-exchange electron transfer integral calculated from A–D–A trimer; (b) super-exchange hole transfer calculated from D–A–D trimer.

The super-exchange electron (t_e^{super}) and hole (t_h^{super}) transfer integral values in the cocrystal are 45 and 48 meV respectively indicating an ambipolar transport along the mixed π-stack (Figure 10). We have checked the symmetry and energies of the frontier molecular orbitals on perylene and TCNQ to find the origin of ambipolar transport. The HOMO (-4.96 eV) of perylene and the LUMO of TCNQ (-4.81 eV) are energetically closer, and both possess vertical *ungerade* symmetry (Figure 11a). Hence, the LUMO of the TCNQ molecule acts as the bridging orbital for the super-exchange hole transport from the HOMO of one perylene molecule to the HOMO of perylene molecule (Figure 11b). Similarly, the HOMO of perylene molecule acts as the bridging orbital for the electron transport from the LUMO of one TCNQ molecule to the LUMO of consecutive TCNQ molecule (Figure 11b). We have shown the importance of bridging HOMO-1 orbital on the donor in super-exchange mediated electron transport in our previous study.[15] The HOMO-1 orbital of perylene is energetically much lower (-5.75 eV) than the LUMO of TCNQ (Figure 11a). As a result, this orbital is not supposed to act as the bridging orbital for super-exchange mediated electron transport process in 1:1 perylene:TCNQ cocrystal. The direct hole (t_h^{direct}) and electron

View Article Online
DOI: 10.1039/D6CP00757K

(t_e^{direct}) transfer integrals calculated from the nearest D–D and A–A dimers are 8.5 and 7.0 meV respectively (Figure S8 in SI).

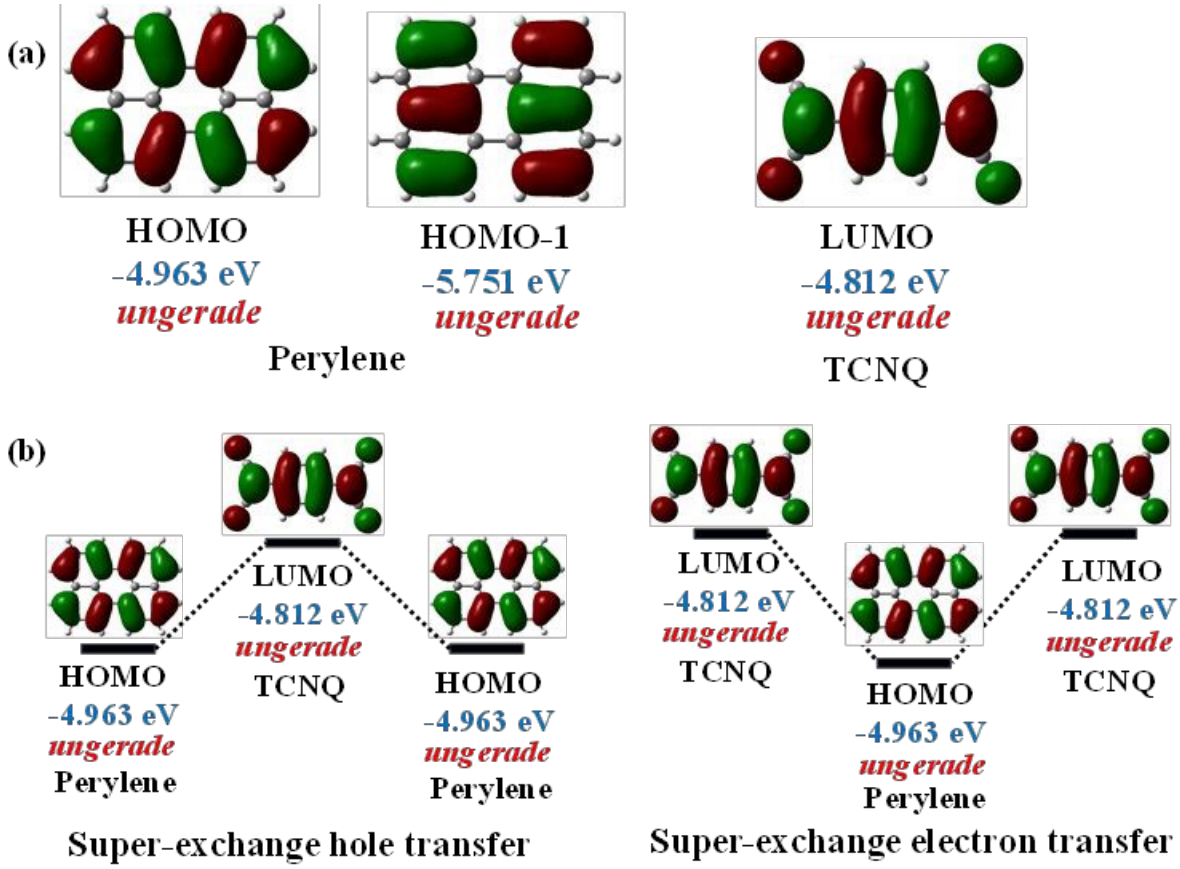

Figure 11. (a) Energy and symmetry of frontier molecular orbitals on perylene and TCNQ calculated at B3LYP/6-31G(d,p) level of theory on optimized gas phase geometries; (b) super-exchange hole and electron transfer processes in 1:1 perylene:TCNQ cocrystal.

We have calculated the internal reorganization energy (λ_{int}) of the perylene and TCNQ moieties from a four point energy model as described in Figure S16. The internal hole reorganization energy of perylene is 147 meV. This small value of λ_{int} corresponds with the minimal changes in the respective C–C and C=C bond-lengths from neutral perylene to perylene radical cation as follows:

C–C and C=C bond-lengths in neutral perylene: 1.430, 1.476, 1.390, 1.375, 1.420, 1.435, 1.433 Å.
C–C and C=C bond-lengths in perylene cation: 1.452, 1.451, 1.392, 1.390, 1.414, 1.430, 1.428 Å.

View Article Online
DOI: 10.1039/D6CP00757K

The C≡N, C–C and C=C bond-lengths in the optimized neutral and anionic geometries of TCNQ are listed. The C≡N bond-lengths in optimized neutral and anionic geometries of TCNQ are 1.165 and 1.170 Å respectively. The C–C and C=C bond-lengths in the optimized geometry of TCNQ: 1.427, 1.390, 1.447, 1.355 Å. The respective C–C and C=C bond-lengths found in the anionic radical geometry of TCNQ: 1.416, 1.432, 1.425, 1.375 Å (Table S3 in SI). The change in bond-lengths in TCNQ upon ionization is more prominent than that observed for the ionization in perylene, and this explains the higher value of λ_{int} (255 meV) for TCNQ in comparison to perylene. The internal electron reorganization energy value of TCNQ from our calculation matches well with the value (250 meV) reported in the literature.[69] The comparison of electron and hole transport rates in perylene:TCNQ cocrystal was done by considering an activationless transport process[70] *i.e.*, the free energy of charge carrier transport $\Delta G^{\neq} = 0$.

As the $\Delta G^{\neq} = \Delta G° + \lambda = 0$, the $\Delta G° = -\lambda$ and the rate of charge carrier transfer,

$$k_T = \frac{4\pi^2}{h}\frac{1}{\sqrt{4\pi\lambda k_B T}}t^2 \text{ as } exp(0) = 1.$$

The ratio of rate of the hole and electron transfer rates, $k^h_T/k^e_T = [(48+8.5)^2/\sqrt{147}]/[(45+7)^2/\sqrt{255}] = 1.55$, considering the super-exchange and direct electron and hole transfer integral values, and the internal hole reorganization energy of perylene and the internal electron reorganization energy of TCNQ. This implies that the perylene:TCNQ cocrystal is an ambipolar charge carrier material. It is pertinent to note that 1:1 perylene:TCNQ cocrystal system was deemed as an *n*-type semiconductor from experimental mobility value measurements in the literature.[41a,41c] In contrast, this cocrystal was found as an ambipolar semiconductor from DFT calculations by us and others.[41b] We are not sure of the origin of disparity between theoretical and experimental results.

We have also estimated the internal and external components of the total reorganization energy using QM/MM model. The unit cell was fully relaxed in both the neutral and charged optimized states producing the $E^N_{geom=N}$ and $E^C_{geom=C}$ terms of the total reorganization energy. One perylene or one TCNQ molecule was considered in the QM layer and at B3LYP/6-31G(d,p) level of theory, while other molecules were considered within the MM layer at universal force field (UFF) with the polarization embedding and charge equilibration (QEq).[71] The terms $E^C_{geom=N}$ and $E^N_{geom=C}$ denote single point charged total energy carried out at the optimized neutral geometry, and single point neutral total energy carried out at the optimized charged geometries, respectively. The total reorganization energy λ^{tot} (*i.e.*, $\lambda^{int} + \lambda^{ext}$) is calculated following the four point energy model: $\lambda^{tot} = 1/2 \times (E^C_{geom=N} - E^C_{geom=C} + E^N_{geom=C} - E^N_{geom=N})$ Equation (5)[72]

View Article Online
DOI: 10.1039/D6CP00757K

The external reorganization energy of 1:1 perylene:TCNQ cocrystal is only 12 meV using universal force field for the MM region and one TCNQ molecule in the QM region, in contrast, the value of externa reorganization energy is 49.8 meV using universal force field for the MM region and one perylene molecule in the QM layer. These values indicate that the perylene:TCNQ cocrystal has low external reorganization energy which is favourable for charge carrier transport since thermal energy loss is expected to be small. The difference in the external reorganization energy value when calculated using TCNQ or perylene can be explained by the relative size of the two molecules and their effect in packed crystal structure. The larger size of perylene molecule is expected to have more prominent effect on the neighbouring molecules compared to the effect exerted by small sized TCNQ molecule.

Band structure analysis of perylene:TCNQ cocrystal

The band structure of perylene:TCNQ cocrystal was calculated with both the generalized gradient approximation (GGA) PBE functional and the HSE06 hybrid functional at the experimental unit cell and optimized geometries. The hybrid exchange-correlation functional HSE06 is in general considered to be more accurate for bandgap calculations in comparison to most DFT functionals. However, the HSE06 functional is still reported to under-estimates the bandgap value with an mean error of typically 0.2-0.25 eV.[73]

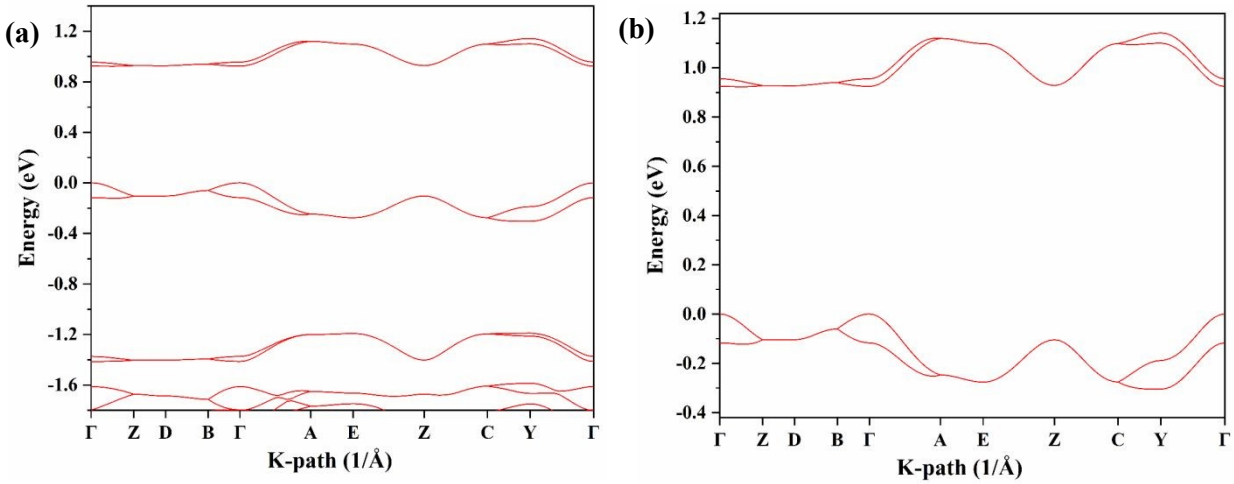

Figure 12. (a) Band structure of 1:1 perylene:TCNQ cocrystal calculated on experimental geometry with hybrid HSE06 functional using Monkhorst-pack 5×3×2 mesh of k-points and 500 eV energy cut-off and Gaussian smearing; (b) the bands near VBM and CBM are shown.

View Article Online
DOI: 10.1039/D6CP00757K

The band structure is plotted along the high symmetry points in the first Brillouin zone (Figure 12a), and the coordinates of high symmetry points of the first Brillouin zone are listed in Table S4 in SI. The perylene:TCNQ is an indirect bandgap semiconductor with the valence bond maxima residing at the high symmetry Γ (0, 0, 0) point while the conduction band minima (0, 0.25, 0) is not a high symmetry point (Figure 12 and S10 in SI). The calculated bandgap values of the cocrystal with HSE06 functional on the experimental and optimized unit geometries are 0.92 and 0.91 eV. In contrast, the bandgap calculated with GGA functional PBE is considerably smaller with the value being only 0.25 eV (Figure 12b). Two noticeable curvatures are found in the valence and conduction bands, *viz*. along the B (0, 0, 0.5) → A (-0.5, 0, 0.5) direction indicating the crystallographic *a* axis, and along the E (-0.5, 0.5, 0.5) → C (-0.5, 0.5, 0) direction indicating the crystallographic *c* axis respectively (Figure 12). The first one is the direction of π···π stacking between the donor and acceptor, *i.e*., the direction of super-exchange electron or hole transfer. The second curvature along the crystallographic *c* axis does not indicate any non-covalent interaction bonded chain of donor or acceptor molecules, but rather the close proximity of the neighbouring donor or acceptor molecules along the *c* axis (Figure 13).

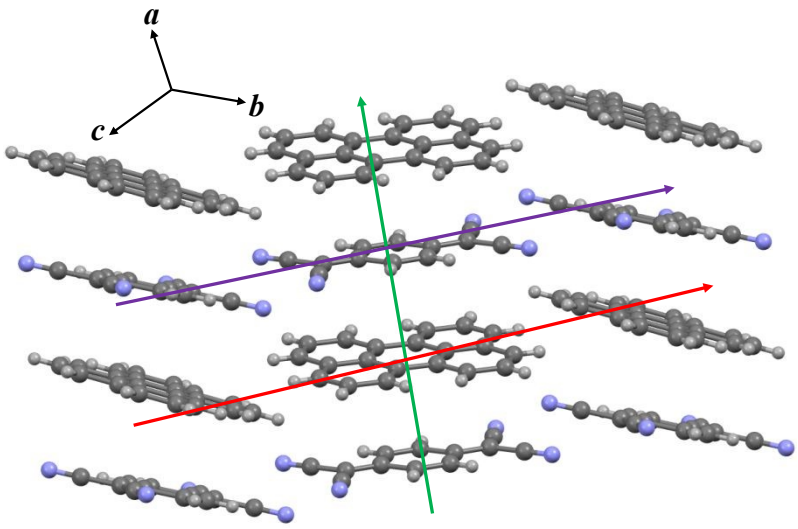

Figure 13. Different directions of electron and hole transport in 1:1 perylene:TCNQ cocrystal: (**1**) super-exchange electron/ hole transfer, (**2**) direct electron transfer, (**3**) direct hole transfer.

The optical bandgap of 1:1 perylene:TCNQ cocrystal calculated from the Tauc plot is 0.80 eV (Figure 14a) considering an indirect optical bandgap material according to the equation:

View Article Online
DOI: 10.1039/D6CP00757K

$(\alpha h\upsilon)^{1/2} = h\upsilon - E_g$ Equation (6);

while α is the absorption coefficient and $h\upsilon$ is the photon energy. The $S_0 \rightarrow S_1$ (E = 1.52 eV), $S_0 \rightarrow S_2$ (E = 2.70 eV), and $S_0 \rightarrow S_3$ (E = 3.20 eV) transitions are clearly observed in the Tauc plot. The oscillator strength of $S_0 \rightarrow S_1$ transition in the NIR region has small value (0.073) compared to the $S_0 \rightarrow S_2$ and $S_0 \rightarrow S_3$ transitions in the visible region, but the oscillator strength (f = 0.07) for the $S_0 \rightarrow S_1$ transition is not negligible leading to absorption in the NIR region as can be observed from the Tauc plot. The optical bandgap calculated from the interpolation is 0.80 eV considering an indirect optical bandgap. The exciton binding energy (E_b) of the cocrystal is calculated from the difference between the optical bandgap and the DFT estimated electronic bandgap. The small value of exciton binding energy (0.12 eV) for Per:TCNQ cocrystal indicates efficient exciton dissociation and potential as organic photovoltaic material. However, this value of exciton binding energy might not be fully accurate by considering the reported under-estimation of electronic bandgap by HSE06 functional. It is pertinent to mention that we have also made a Tauc plot considering direct optical bandgap by following the equation,

$(\alpha h\upsilon)^2 = h\upsilon - E_g$ Equation (7).

The estimated direct optical bandgap is 2.70 eV, however, this bandgap value does not correspond to the absorption features of the cocrystal or to the DFT calculated electronic bandgap value (Figure S11 in SI).

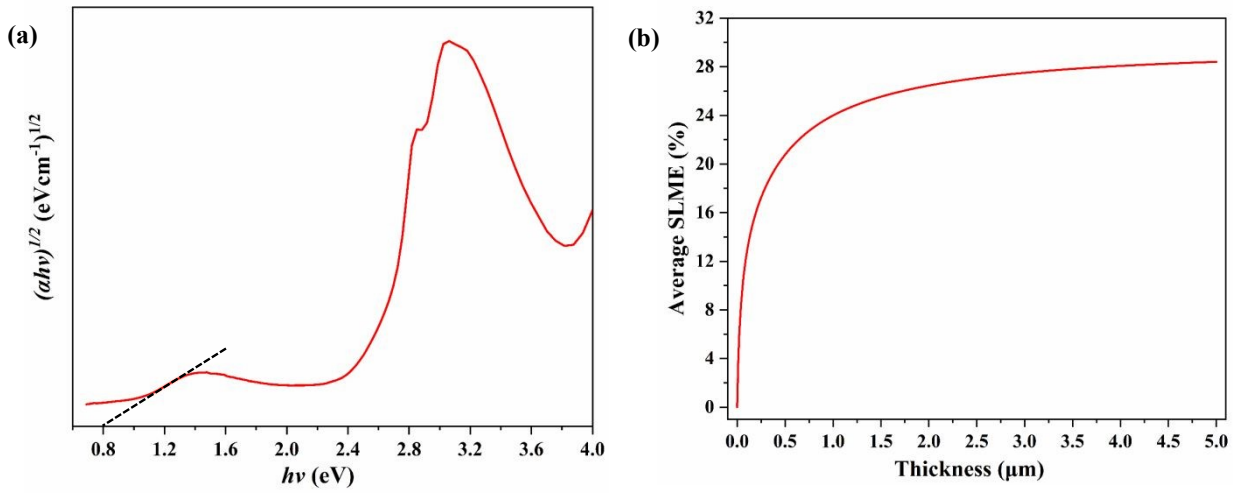

Figure 14. (a) Tauc plot of 1:1 perylene:TCNQ cocrystal considering indirect optical bandgap; (b) spectroscopic limited maximal efficiency (SLME) calculated using experimental unit cell

View Article Online
DOI: 10.1039/D6CP00757K

geometry, HSE06 functional, 500 eV energy cut-off, Gaussian smearing, and Monkhorst-pack 5×3×2 mesh of k-points.

To understand the potential of the 1:1 perylene:TCNQ cocrystal as a photovoltaic material, we have calculated the 'spectroscopy limited maximum efficiency' (SLME) parameter proposed by Yu and Zunger from the periodic DFT study.[76] The SLME value calculation was performed by using the VASPKIT's optical property evaluation tools.[77] The SLME parameter indicates the maximum theoretical photo-conversion efficiency of a material. The cocrystal shows a SLME value of 24 % at a thin film thickness 1000 nm, which indicates remarkable theoretical photo-conversion efficiency for an organic semiconductor. This high SLME value at lower thin film thickness is surprising for an indirect bandgap material, and, in part is a direct consequence of the values of the fundamental bandgap (0.92 eV) and the direct allowed bandgap (0.93 eV) being very similar. The high SLME value of the 1:1 perylene:TCNQ cocrystal is also attributed to the system absorbing both in the visible and NIR region. The SLME parameter takes account of a material's absorption in standard AM 1.5 G solar spectrum which spans from 280-2000 nm (0.62-4.42 eV) range. The 1:1 perylene:TCNQ system shows absorption spanning from 325-1150 nm (1.08-3.82 eV), and utilizes a wide range of AM 1.5 G solar spectrum to have high SLME value.

To understand the relation between the band structure features and the SLME values, we have investigated the optical properties of two reported semiconductor D–A cocrystals (Figure S12 in SI) *viz.* 1:1 1-aminopyrene:TCNQ and 1:2 CBP:$(TCNQ)_2$ (CBP = π-donor 4,4′-bis(carbazol-9-yl)biphenyl) with electron dominant transport features.[78-79] Both the 1-minopyrene:TCNQ and CBP:$(TCNQ)_2$ corystals have indirect bandgap. The cocrystal 1-aminopyrene:TCNQ shows spectroscopic limited maximal efficiency value 23 % at thin film thickness 1000 nm, while the fundamental bandgap and the direct allowed bandgap values for the cocrystal are 0.81 and 0.85 eV respectively. Similarly, the CBP:$(TCNQ)_2$ cocrystal shows the SLME value 29 % at thin film thickness 1000 nm with the fundamental bandgap and the direct allowed bandgap values being 0.92 and 0.97 eV respectively. The direct bandgap materials are known for efficient photon absorption even at low material thickness, resulting in high SLME values. In contrast, the indirect bandgap materials does not absorb photon efficiently at low material thickness, and this causes low SLME values. In contrast, achieving high SLME value with low thin film thickness is possible for the indirect bandgap organic materials if the difference between the fundamental bandgap and the direct allowed bandgap is considerably small, as this will help to minimize the non-radiative

View Article Online
DOI: 10.1039/D6CP00757K

recombination pathways.[75] The commercial indirect bandgap semiconductor materials Cs_3AlTe_3 and Cu_3TlS_2 have SLME values nearly 25 %. The difference between the indirect bandgap and direct allowed bandgap in Cs_3AlTe_3 is 0.07 eV, and this difference is 0.14 eV for Cu_3TlS_2.[75] The difference between the indirect bandgap and direct allowed bandgap is ≤ 0.05 eV in our studied cocrystals, which leads to higher SLME values for these systems.

It is pertinent to mention that the SLME parameter considers photon absorption, exciton generation and dissociation and recombination processes. It is not related to the electron and hole transport processes. Transport of electron and hole to the electrodes is a major factor deciding the actual photo-conversion efficiency. The efficiency of a photovoltaic device does not only depend on the optical property of the material, but also on its charge carrier transport properties and device fabrication conditions like thin film engineering, electrode material and dimensions *etc*. Hence, the SLME value gives a good estimation of the theoretical maximum photo-conversion efficiency, but not the true efficiency of a photovoltaic device. We have discussed electron and hole transport pathways and corresponding transfer integral values in this study. However, the device fabrication is out of scope of this theoretical study.

Conclusion

In this work, we have elucidated the photo-physical and charge carrier transport features of 1:1 cocrystal of perylene donor and 7,7′,8,8′-tetracyanoquinodimethane (TCNQ) acceptor with infinite π-stacked chains of the alternative donor and acceptor molecules. This cocrystal is characterized with strong charge transfer from the perylene to TCNQ moiety, which leads to absorption in the far red and near infra-red region of solar spectrum. The electronic bandgap of the cocrystal (0.92 eV), small value of the exciton binding energy (0.12 eV), and the prominent electron-hole geometric offset in the optical excited states with significant distance between the epicenters of electron and hole are indicative of efficient photon absorption, exciton generation and dissociation. The 1:1 perylene:TCNQ cocrystal is recognized as an ambipolar semiconductor with significant values of the super-exchange electron (45meV) and hole (48 meV) transfer integrals along the π-stacked ··D–A–D–A·· chain. Low values of internal hole reorganization energy of perylene (147 meV) and TCNQ (255 meV) are conducive to fast charge transport and low thermal energy loss, in addition this system also shows very low value for the external reorganization energy.

View Article Online
DOI: 10.1039/D6CP00757K

The cocrystal is characterized with an indirect bandgap, however, it still shows high value (24 %) of 'spectroscopic limited maximal efficiency' (SLME) at 1000 nm thin film thickness suitable for thin film photovoltaic application. This intriguing feature of high theoretical photo-conversion efficiency is intimately linked with the very similar values of fundamental bandgap and direct allowed bandgap and consequently suppressing the non-radiative recombination pathways. This illustrates that achieving high value of theoretical photo-conversion efficiency at low thin film thickness with indirect bandgap organic semiconductor is possible. This fact was further supported by the calculating SLME for two reported semiconductor D–A cocrystals 1-aminopyrene:TCNQ and CBP:$(TCNQ)_2$ with indirect bandgaps. Both these cocrystals have very similar values of the fundamental bandgap and the direct allowed bandgap, and show SLME values over 20 % at 1000 nm thin film thickness. The current study explores the opto-electronic features of a sustainable D–A cocrystal that can be easily synthesized and solution processed at ambient conditions pointing towards promising avenues for the implementation within photovoltaic devices. Additionally, this study elucidates how detailed features of the band structures impact the theoretical photo-conversion efficiency. Mostly organic semiconductors with direct bandgap have been studied in details. Our study first elucidated the scope of organic semiconductors with indirect bandgap for photovoltaic application. The D–A organic cocrystals showed immense potential as an ambipolar or *n*-type molecular semiconductors, and the present study unravels their potential for the solution processible, thin film molecular photovoltaics.

Acknowledgement

This work has received funding from the European Union's Horizon Europe research and innovation programme under the Marie Skłodowska-Curie grant agreement No 101106582, and Growth House of University of Oslo grant agreement No 15300500/102419163. Computational resources have been available from the Norwegian infrastructure for high-performance computing (NOTUR) through a grant of computing time (grant number NN2916K). AM is thankful to Dr. Javier Carmona Garcia from School of Chemistry, University of Bristol for useful discussions.

Author contribution

View Article Online
DOI: 10.1039/D6CP00757K

AM: Conceptualizing the project, structural and DFT studies, writing the main draft, acquiring funding; **CEM**: DFT calculations, editing manuscript, acquiring of funding; **CHG**: contribution to describing the molecular structure; **YC**: acquiring and interpreting the absorption spectrum.

Supporting information for publication

Table S1: Crystallographic and refinement table; figure S1: *ORTEP* diagram of perylene:TCNQ, figure S2: formation of perylene:TCNQ; figure S3-S6: molecular orbital description of π-stacked dimer and tetramer, and hexamer in perylene:TCNQ; table S2 and figure S7: time dependent DFT (TD-DFT) calculations on π-stacked dimer in perylene:TCNQ; table S3: bond-lengths in neutral and anionic TCNQ; S8: direct electron and hole transfer integral in perylene:TCNQ; figure S9: calculated absorption spectra by periodic DFT of perylene:TCNQ; table S4: coordinates of high symmetry points of perylene:TCNQ; figure S10: band structure of perylene:TCNQ calculated using PBE functional; table S5: coordinates of high symmetry points of 1-aminopyrene:TCNQ and CBP:$(TCNQ)_2$; figure S11: fitting Tauc plot for direct bandgap of perylene:TCNQ; figure S12: unit cell of 1-aminopyrene:TCNQ and CBP:$(TCNQ)_2$ cocrystals; figure S13: band structure, calculated absorption spectrum and SLME of 1-aminopyrene:TCNQ; figure S14: band structure, calculated absorption spectrum and SLME of CBP:$(TCNQ)_2$.

References:

1. A. W. Hains, Z. Liang, M. A. Woodhouse, B. A. Gregg, Molecular semiconductors in organic photovoltaic cells, *Chem. Rev.*, 2010, 110, 11, 6689–6735.

2. C. M. Aitchison, I. McCulloch, Organic Photovoltaic Materials for Solar Fuel Applications: A Perfect Match?, *Chem. Mater.*, 2024, 36, 4, 1781–1792.

3. W. C. Su, C. C. Lee, Y. Z. Li, and S. W. Liu, Influence of Singlet and Charge-Transfer Excitons on the Open-Circuit Voltage of Rubrene/Fullerene Organic Photovoltaic Device, *ACS Appl. Mater. Interfaces*, 2016, 8, 28757−28762.

4. M. W. B. Wilson, A. Rao, B. Ehrler, and R. H. Friend, Singlet Exciton Fission in Polycrystalline Pentacene: From Photophysics toward Devices, *Acc. Chem. Res.*, 2013, 46, 6, 1330–1338.

5. S. D. Oosterhout, V. Savikhin, J. Zhang, Y. Zhang, M. A. Burgers, S. R. Marder, G. C. Bazan, and M. F. Toney, Mixing Behavior in Small Molecule:Fullerene Organic Photovoltaics, *Chem. Mater.*, 2017, 29, 3062−3069.

View Article Online
DOI: 10.1039/D6CP00757K

6. J. Qian, S. Jiang, S. Li, X. Wang, Y. Shi, and Y. Li, Solution-Processed 2D Molecular Crystals: Fabrication Techniques, Transistor Applications, and Physics, *Adv. Mater. Technol*., 2019, 4, 1800182.

7. A. F. Eftaiha, J. P. Sun, I. G. Hill, and G. C. Welch, Recent advances of non-fullerene, small molecular acceptors for solution processed bulk heterojunction solar cells, *J. Mater. Chem. A*, 2014, 2, 1201-1213.

8. W. Chen, and Q. Zhang, Recent progress in non-fullerene small molecule acceptors in organic solar cells (OSCs), *J. Mater. Chem. C*, 2017, 5, 1275-1302.

9. J. Zhang, H. S. Tan, X. Guo, A. Facchetti, H Yan, Material insights and challenges for non-fullerene organic solar cells based on small molecular acceptors, *Nat. Energy*, 2018, 3, 720-731.

10. A. Armin, W. Li, O. J. Sandberg, Z. Xiao, L. Ding, J. Nelson, D. Neher, K. Vandewal, S. Shoaee, T. Wang, H. Ade, T. Heumüller, C. Brabec, and P. Meredith A History and Perspective of Non-Fullerene Electron Acceptors for Organic Solar Cells, *Adv. Energy Mater*., 2021, 11, 20003570.

11. M. Kim, S. U. Ryu, S. A. Park, Y. J. Pu, and T. Park, Designs and understanding of small molecule-based non-fullerene acceptors for realizing commercially viable organic photovoltaics, *Chem. Sci.*, 2021, 12, 14004–14023.

12. M. M. Mandoc, F. B. Kooistra, J. C. Hummelen, B. de Boer, P. W. M. Blom, Effect of traps on the performance of bulk heterojunction organic solar cells, *Appl. Phys. Lett.*, 2007, 91, 263505.

13. S. R. Cowan, N. Banerji, W. L. Leong, and A. J. Heeger, Charge Formation, Recombination, and Sweep-Out Dynamics in Organic Solar Cells, *Adv. Funct. Mater*., 2012, 22, 1116–1128.

14. H. Zhang, L. Jiang, Y. Zhen, J. Zhang, G. Han, X. Zhang, X. Fu, Y. Yi, W. Xu, H. Dong, W. Chen, W. Hu, and D. Zhu, Organic Cocrystal Photovoltaic Behavior: A Model System to Study Charge Recombination of C60 and C70 at the Molecular Level, *Adv. Electron. Mater*., 2016, 2, 1500423.

15. A. Mandal, C. E. Mohn, C. H. görbitz, and A. Roy, Cocrystal Engineering of Organic Semiconductors for Photovoltaic Applications: Modeling Excited-State Properties of a Charge Transfer Cocrystal of a Dicarbazole Donor and a Fluoranil Acceptor, *J. Phys. Chem. C*, 2026, 130, 2, 882-897.

View Article Online
DOI: 10.1039/D6CP00757K

16. N. Yee, A. Dadvand, and D. F. Perepichka, Band gap engineering of donor–acceptor co-crystals by complementary two-point hydrogen bonding, *Mater. Chem. Front*., 2020, 4, 3669-3677.

17. S. Li, L. Zheng, Y. Chan, B. Li, Y. Sun, L. Sun, C. Zhen, X. Zhang, and W. Hu, An organic cocrystal based on phthalocyanine with ideal packing mode towards high-performance ambipolar property, *J. Mater. Chem. C*, 2022, 10, 9596-9601.

18. P. Yu, Y. Li, H. Zhao, L. Zhu, Y. Wang, W. Xu, Y. Zhen, X. Wang, H. Dong, D. Zhu, W. Hu, 1D Mixed-Stack Cocrystals Based on Perylene Diimide toward Ambipolar Charge Transport, *Small*, 2021, 17, 2006574.

19. W. Wang, L. Luo, Z. Lin, Z. Mu, Z. Ju, B. Yang, Y. Li, M. Lin, G. Long, J. Zhang, J. Zhao, W. Huang, Cocrystal engineering of molecular rearrangement: a "turn-on" approach for high-performance N-type organic semiconductors, *J. Mater. Chem. C*, 2021, 9, 7928-7935.

20. R. Sato, T. Kawamoto, and T. Mori, Asymmetrical hole/electron transport in donor–acceptor mixed-stack cocrystals, *J. Mater. Chem. C*, 2019, 7, 567-577.

21. J. H. Lee, D. H. Lee, H. J. Kim, S. Choi, G. E. Park, M. J. Cho, D. H. Choi, Ambipolar Charge Transport in a Donor–Acceptor–Donor-Type Conjugated Block Copolymer and Its Gate-Voltage-Controlled Thin Film Transistor Memory, *J. Polym. Sci. Part A: Polym. Chem.*, 2017, 55, 3223–3235.

22. J. Lee, A. R. Han, H. Yu, T. J. Shin, C. Yang, and J. H. Oh, Boosting the Ambipolar Performance of Solution-Processable Polymer Semiconductors via Hybrid Side-Chain Engineering, *J. Am. Chem. Soc*., 2013, 135, 9540−9547.

23. J. Zhang, H. Geng, T. S. Virk, Y. Zhao, J. Tan, C. Di, W. Xu, K. Singh, W. Hu, Z. Shuai, Y. Liu, and D. Zhu, Sulfur-Bridged Annulene-TCNQ Co-Crystal: A Self-Assembled "Molecular Level Heterojunction" with Air Stable Ambipolar Charge Transport Behavior, *Adv. Mater*., 2012, 24, 2603–2607.

24. A. Mandal, A. Choudhury, S. Sau, P. K. Iyer, and P. Mal, Exploring Ambipolar Semiconductor Nature of Binary and Ternary Charge-Transfer Cocrystals of Triphenylene, Pyrene, and TCNQ, *J. Phys. Chem. C*, 2020, 124, 12, 6544–6553.

25. W. R. Bodlos, S. K. Park, B. Kunert, S. Y. Park, and R. Resel, Thin Film Growth of a Charge Transfer Cocrystal (DCS/TFPA) for Ambipolar Thin Film Transistors, *ACS Appl. Electron. Mater*., 2021, 3, 2783−2789.

View Article Online
DOI: 10.1039/D6CP00757K

26. Y. Su, Y. Li, J. Liu, R. Xing, and Y. Han, Donor–acceptor cocrystal based on hexakis(alkoxy)triphenylene and perylenediimide derivatives with an ambipolar transporting property, *Nanoscale*, 2015, 7, 1944–1955.

27. G. Gao, M. Chen, J. Roberts, M. Feng, C. Xiao, G. Zhang, S. Parkin, C. Risko, and L. Zhang Rational Functionalization of a C70 Buckybowl To Enable a C70:Buckybowl Cocrystal for Organic Semiconductor Applications, *J. Am. Chem. Soc.*, 2020, 142, 5, 2460–2470.

28. W. Sun, Y. Zheng, K. Yang, Q. Zhang, A. A. Shah, Z. Wu, Y. Sun, L. Feng, D. Chen, Z. Xiao, S. Lu, Y. Li, K. Sun, Machine learning–assisted molecular design and efficiency prediction for high-performance organic photovoltaic materials, *Sci. Adv.*, 2019, 5, eaay4275.

29. J. Roncali, P. Leriche, P. Blanchard, Molecular Materials for Organic Photovoltaics: Small is Beautiful, *Adv. Mater.*, 2014, 26, 3821-3838.

30. T. Salzillo, M. Masino, G. K. Köhn, D. D. Nuzzo, E. Venuti, R. G. D. Valle, D. Vanossi, C. Fontanesi, A. Girlando, A. Brillante, and E. D. Como, Structure, Stoichiometry, and Charge Transfer in Cocrystals of Perylene with TCNQ-Fx, *Cryst. Growth Des.*, 2016, 16, 3028−3036.

31. T. Salzillo, R. G. Della Valle, E. Venuti, G. K. Köhn, M. Masino, A. Girlando, A. Brillante, Solution equilibrium between two structures of Perylene-F_2TCNQ charge transfer co-crystals, *J. Cryst. Growth*, 2019, 516, 45-50.

32. J. Guo, L. Xu, M. Cai, Z. Dong, Q. Mu, X. Wang, H. Fan, F. Teng, X. He, H. Jiang, and P. Hu, Crystal Growth, Intermolecular Noncovalent Interactions, and Photoluminescence Properties of Halogenated Phthalic Anhydride-Based Organic Charge Transfer Cocrystals, *Cryst. Growth Des.*, 2024, 24, 1293−1301.

33. J. Zhang, J. Chen, B. Yang, S. Ma, L. Yin, Z. Liu, W. Xiang, H. Liu, J. Zhao, and P. Sheng, Energy Level, Crystal Morphology and Fluorescence Emission Tuning in Cocrystals via Molecular-Level Engineering, *Chem. Eur. J.*, 2023, 29, e202202915.

34. J. Li, S. Takaishi, N. Fujinuma, K. Endo, M. Yamashita, H. Matsuzaki, H. Okamoto, K. Sawabe, T. Takenobu, and Y. Iwasa, Enhancement of luminescence intensity in TMPY/perylene co-single crystals, *J. Mater. Chem.*, 2011, 21, 17662–17666.

35. A. Ashokan, C. Hanson, N. Corbin, J. L. Brédas, and V. Coropceanu, Electronic, vibrational, and charge-transport properties of benzothienobenzothiophene-TCNQ co-crystals, *Mater. Chem. Front.*, 2020, 4, 3623-3631.

View Article Online
DOI: 10.1039/D6CP00757K

36. Q. Ai, Y. A. Getmanenko, K. Jarolimek, R. Castañeda, T. V. Timofeeva, and C. Risko, Unusual Electronic Structure of the Donor−Acceptor Cocrystal Formed by Dithieno[3,2-a:2′,3′-c]phenazine and 7,7,8,8-Tetracyanoquinodimethane, *J. Phys. Chem. Lett*., 2017, 8, 4510−4515.

37. S. Melis, S. Hung, C. Bagade, Y. Chung, E. Hughes, X. Zhang, P. Barbara, P. Han, T. Li, D. McCusker, R. Hartsmith, J. Bertke, P. Dev, I. Stone, J. Joshi, P. Vora, and E. V. Keuren, Charge Transport through Superexchange in Phenothiazine−7,7,8,8-Tetracyanoquinodimethane (PTZ−TCNQ) Cocrystal Microribbon FETs Grown Using Evaporative Alignment, *ACS Appl. Electron. Mater.*, 2022, 4, 12, 5973–5983.

38. R. Ramanathan, L. L. Martin, A. M. Bond, V. Bansal, Emerging Applications of TCNQ-Based Metal–Organic Semiconducting Materials, *ACS Appl. Nano Mater.*, 2024, 7, 24, 28057–28073.

39. C. Schneider, D. Ukaj, R. Koerver, A. A. Talin, G. Kieslich, S. P. Pujari, H. Zuilhof, J. Janek, M. D. Allendorf, and R. A. Fischer, High electrical conductivity and high porosity in a Guest@MOF material: evidence of TCNQ ordering within Cu_3BTC_2 micropores, *Chem. Sci*., 2018, 9, 7405–7412.

40. (a) I. J. Tickle and C. K. Prout, Molecular Complexes. Part XVII[1] Crystal and Molecular Structure of Perylene-7,7,8,8-Tetracyanoquinodimethane Molecular Complex, *J. Chem. Soc., Perkin Trans.* 2, 1973, 2, 720-723; (b) J. Henderson, M. Masino, L. E. Hatcher, G. Kociok-Köhn, T. Salzillo, A. Brillante, P. R. Raithby, A. Girlando, and E. D. Como, New Polymorphs of Perylene:Tetracyanoquinodimethane Charge Transfer Cocrystals, *Cryst. Growth Des*., 2018, 18, 2003−2009.

41. (a) R. Sanada, D. Yoo, R. Sato, K. Iijima, T. Kawamoto, and T. Mori, Ambipolar Transistor Properties of Charge-Transfer Complexes Containing Perylene and Dicyanoquinonediimines, *J. Phys. Chem. C*, 2019, 123, 12088−12095; (b) D. Vermeulen, L. Y. Zhu, K. P. Goetz, Peng Hu, Hui Jiang, C. S. Day, O. D. Jurchescu, V. Coropceanu, C. Kloc, and L. E. McNeil, Charge Transport Properties of Perylene−TCNQ Crystals: The Effect of Stoichiometry, *J. Phys. Chem. C*, 2014, 118, 24688−24696; (c) H. D. Wu, H. D. Peng, and G. B. Pan, Precise growth of low-dimensional pyrene·perylene·TCNQ co-crystals and structure–property related optoelectronic properties, *RSC Adv.*, 2016, 6, 78979-78983.

42. S. F. Boys, F. Bernardi, The calculation of small molecular interactions by the differences of separate total energies. Some procedures with reduced errors, *Mol. Phys*., 1970, 19, 553-566.

View Article Online
DOI: 10.1039/D6CP00757K

43. C. F. Mackenzie, P. R. Spackman, D. Jayatilaka, M. A. Spackman, *CrystalExplorer* model energies and energy frameworks: extension to metal coordination compounds, organic salts, solvates and open-shell systems, *IUCrJ*, 2017, 4, 575-587.

44. P. R. Spackman, M. J. Turner, J. J. McKinnon, S. K. Wolff, D. J. Grimwood, D. Jayatilaka, M, A. Spackman, *J. Appl. Cryst*., 2021, 54, 1006-1011.

45. S. Grimme, Density functional theory with London dispersion corrections, *WIREs Comput. Mol. Sci.*, 2011, 1, 211-228.

46. S. Grimme, S. Ehrlich, L. Goerigk, Effect of the damping function in dispersion corrected density functional theory, *Comput. Chem*., 2011, 32, 1456-1465.

47. F. Weinhold, C.R. Landis, E.D. Glendening, What is NBO analysis and how is it useful? *International Reviews in Physical Chemistry*, 2016, 35, 399-440.

48. A. E. Reed, L. A. Curtiss, F. Weinhold, Intermolecular Interactions from a Natural Bond Orbital, Donor-Acceptor Viewpoint, *Chem. Rev*., 1988, 88, 899-926.

49. K. Okuno, Y. Shigeta, R. Kishi, M. Nakano, Non-empirical tuning of CAM-B3LYP functional in time-dependent density functional theory for excitation energies of diarylethene derivatives, *Chem. Phys. Lett*., 2013, 585, 201-206.

50. M. Li, J. R. Reimers, M. J. Ford, R. Kobayashi, R. D. Amos, Accurate prediction of the properties of materials using the CAM-B3LYP density functional, *J. Comput. Chem*., 2021, 42, 1486-1497.

51. T. Lu, A comprehensive electron wavefunction analysis toolbox for chemists, Multiwfn, *J. Chem. Phys.*, 2024, 161, 082503.

52. T. Lu, F. Chen, Multiwfn: A multifunctional wavefunction analyzer, *J. Comput. Chem*., 2012, 33, 580-592.

53. Y. Li, C.A. Ullrich, Time-dependent transition density matrix, *Chem. Phys*., 2011, 391, 157-163.

54. C. H. Moore, P. Jena, J. T. McLeskey Jr, Tuning range-separated DFT functionals for modeling the peak absorption of MEH-PPV polymer in various solvents, *Comput. Theor. Chem*., 2019, 1162, 112506.

55. O. L. Estrada, H. G. Laguna, C. B. Flores, C. A. Bedolla, Reassessment of the Four-Point Approach to the Electron-Transfer Marcus−Hush Theory, *ACS Omega*, 2018, 3, 2130-2140.

View Article Online
DOI: 10.1039/D6CP00757K

56. A. V. Krukau, O. A. Vydrov, A. F. Izmaylov, and G. E. Scuseria, Influence of the exchange screening parameter on the performance of screened hybrid functionals, *J. Chem. Phys*., 2006, 125, 224106.

57. S. Adhikari, J. Clary, R. Sundararaman, C. Musgrave, D. V. Fowler, C. Sutton, Accurate Prediction of HSE06 Band Structures for a Diverse Set of Materials Using Δ-Learning, *Chem. Mater.*, 2023, 35, 20, 8397-8405.

58. K. Choudhary, M. Bercx, J. Jiang, R. Pachter, D. Lamoen, F. Tavazza, Accelerated Discovery of Efficient Solar Cell Materials Using Quantum and Machine-Learning Methods, *Chem. Mater*., 2019, 31, 5900-5908.

59. M. D. Shavez, A. N. Panda, Assessing Effects of Different π bridges on Properties of Random Benzodithiophene-thienothiophene Donor and Non-fullerene Acceptor Based Active Layer, *J. Phys. Chem. A*, 2021, 125, 9852-9864.

60. S. Kraner, R. Scholz, F. Plasser, C. Koerner, K. Leo, Exciton size and binding energy limitations in one-dimensional organic materials, *J. Chem. Phys.*, 2015, 143, 244905.

61. R. A. Marcus, Tutorial on rate constants and reorganization energies, *J. Electroanalytical Chemistry*, 2000, 483, 2-6.

62. L. Zhu, Y. Yi, Y. Li, E.-G. Kim, V. Coropceanu and J.-L. Brédas, Prediction of remarkable ambipolar charge-transport characteristics in organic mixed-stack charge-transfer crystals, *J. Am. Chem. Soc*., 2012, 134, 2340-2347.

63. B. Liu, S. Fan, R. Huang, T. Kawamoto, T. Mori, Transistor Properties of Charge-Transfer Complexes–Combined Requirements from Energy Levels and Orbital Symmetry, *J. Phys. Chem. C*, 2023, 127, 5125-5133.

64. K. Iijima, R. Sanada, D. Yoo, R. Sato, T. Kawamoto, T. Mori, Carrier charge polarity in mixed-stack charge-transfer crystals containing dithienobenzodithiophene, *ACS Appl. Mater. Interfaces*, 2018, 10, 12, 10262-10269.

65. J. Zhang, W. Xu, P. Sheng, G. Zhao, D. Zhu, Organic Donor−Acceptor Complexes as Novel Organic Semiconductors, *Acc. Chem. Res*., 2017, 50, 1654-1662.

66. K. Senthilkumar; F. C. Grozema; F. M. Bickelhaupt; L. D. A. Siebbeles, Charge transport in columnar stacked triphenylenes: Effects of conformational fluctuations on charge transfer integrals and site energies, *J. Chem. Phys*., 2003, 119, 9809-9817.

View Article Online
DOI: 10.1039/D6CP00757K

67. N. Metri, X. Sallenave, C. Plesse, L. Beouch, P. H. Aubert, F. Goubard, C. Chevrot, G. Sini, Processable star-shaped molecules with triphenylamine core as hole-transporting materials: Experimental and theoretical approach, *J. Phys. Chem. C*, 2012, 116, 5, 3765-3772.

68. M. E. Köse, K. S. Schanze, Prediction of internal reorganization energy in photoinduced electron transfer processes of molecular dyads, *J. Phys. Chem. A*, 2020, 124, 45, 9478–9486.

69. A. Yu. Sosorev, Role of intermolecular charge delocalization and its dimensionality in efficient band-like electron transport in crystalline 2,5-difluoro-7,7,8,8-tetracyanoquinodimethane (F2-TCNQ), *Phys. Chem. Chem. Phys.*, 2017, 19, 25478-25486.

70. T. P. Silverstein, Marcus Theory: Thermodynamics CAN Control the Kinetics of Electron Transfer Reactions, *J. Chem. Educ.*, 2012, 89, 1159−1167.

71. A. K. Rappe, C. J. Casewit, K. S. Colwell, W. A. Goddard III, W. M. Skiff, UFF, a full periodic table force field for molecular mechanics and molecular dynamics simulations, *J. Am. Chem. Soc.*, 1992, 114, 25, 10024–10035.

72. D. P. McMahon, A. Troisi, Evaluation of the External Reorganization Energy of Polyacenes, *J. Phys. Chem. Lett.*, 2010, 1, 941-946.

73. (a) A. J. Garza, G. E. Scuseria, Predicting Band Gaps with Hybrid Density Functionals, *J. Phys. Chem. Lett.* 2016, 7, 20, 4165–4170; (b) C. E. Mohn, H. Fjellvåg, P. Vajeeston, M. Valldor, K. Bergum, Benchmarking Density Functional Theory for Accurate Calculation of Nitride Band Gaps, *J. Chem. Theory Comput*., 2026, 22, 1321−1337.

73. L. Zhu, J. Zhang, Y. Guo, C. Yang, Y. Yi, Z. Wei, Small Exciton Binding Energies Enabling Direct Charge Photogeneration Towards Low-Driving-Force Organic Solar Cells, *Angew. Chem. Int. Ed*., 2021, 60, 15348−15353.

74. A. Sugie, K. Nakano, K. Tajima, I. Osaka, H. Yoshida, Dependence of Exciton Binding Energy on Bandgap of Organic Semiconductors, *J. Phys. Chem. Lett.*, 2023, 14, 50, 11412–11420.

75. L. Yu, A. Zunger, Identification of Potential Photovoltaic Absorbers Based on First-Principles Spectroscopic Screening of Materials, *Phys. Rev. Lett*., 2012, 108, 068701.

76. V. Wang, N. Xu, J.-C. Liu, G. Tang, W.-T. Geng, VASPKIT: A User-friendly Interface Facilitating High-throughput Computing and Analysis Using VASP Code, Computer Physics Communications, 2021, 267, 108033.

View Article Online
DOI: 10.1039/D6CP00757K

78. A. Mandal, Tuning p-type to n-type semiconductor nature by charge transfer cocrystallization: effect of transfer integral *vs.* reorganization energy, *CrystEngComm*, 2022, 24, 2072-2080.
79. A. Mandal, A. Choudhury, R. Kumar, P. K. Iyer, and P. Mal, Exploring the semiconductor properties of a charge transfer cocrystal of 1-aminopyrene and TCNQ, *CrystEngComm*, 2020, 22, 720-727.

View Article Online
DOI: 10.1039/D6CP00757K

Data availability

The following is the supplementary data related to this article: crystallographic parameters of perylene:TCNQ cocrystal, and computational details can be obtained in the ESI† section of online version of the article.